TIME OPTIMIZED SMOOTH TRAJECTORY GENERATION FOR 2DOF AND 3DOF REDUNDANTLY ACTUATED CABLE SUSPENDED PARALLEL ROBOTS

Mudduwa Bathubaralage Lahiru Chaaminda Boralugoda

138533D

Degree of Master of Science

Department of Electronic and Telecommunication Engineering

University of Moratuwa

Sri Lanka

October 2019

TIME OPTIMIZED SMOOTH TRAJECTORY GENERATION FOR 2DOF AND 3DOF REDUNDANTLY ACTUATED CABLE SUSPENDED PARALLEL ROBOTS

Mudduwa Bathubaralage Lahiru Chaaminda Boralugoda

138533D

Thesis submitted in partial fulfillment of the requirements for the degree Master of Science in Electronics and Automation

Department of Electronic and Telecommunication Engineering

University of Moratuwa
Sri Lanka

October 2019

Declaration

I declare that this is my own work and this thesis does not incorporate without acknowledgment any material previously submitted for a Degree or Diploma in any other University or institute of higher learning and to the best of my knowledge and belief it does not contain any material previously published or written by another person except where the acknowledgement is made in the text.

Also, I hereby grant to University of Moratuwa the non-exclusive right to reproduce and distribute my thesis, in whole or in part, in print, in electronic or other medium. I retain the right to use this content in whole or in part in future works (such as articles or books).

Signature : Date:

The above candidate has carried out research for the Masters thesis under my supervision.

Name of the supervisor: Prof. Rohan Munasinghe

Signature of the supervisor: Date:

Abstract

Cable Suspended Parallel Robots (CSPR) are a type of cable driven parallel manipulators (CDPR) that has recently become popular for large workspace operations. They possess many advantages over common parallel robot architectures. They also possess the disadvantage of limited dynamics in motion due to the inability to exert compression and the constant limited downward force, gravity. Further, the redundancy in actuation in planar and spatial robots of certain footprints makes it challenging to determine the cable tensions and suitable dynamics for trajectories.

This thesis introduces an analytical model to circumvent the cable tension determination problem using a concept termed as 'Feasible Acceleration Diagram'. It then designs a novel methodology to generate time optimized point to point straight line trajectories with smooth dynamics for redundantly actuated 2DOF and 3DOF point-mass cable suspended parallel robots while ensuring positive cable tensions. The procedure of determination of kinematics for the trajectory is explained in detail with a test case for the 3DOF 4 cable scenario. Finally, the results obtained are verified by a simulation followed by a numerical method.

Acknowledgements

With immense gratitude I would like to acknowledge the support of the research supervisor Prof. Rohan Munasinghe, and course coordinator Dr. Chamira Edussooriya to make this research a success. I would also like to thank the academic staff of the Electronic and Telecommunication department for the guidance given throughout the academic period.

Finally, I want to thank my beloved wife for the encouragement and the support.

Table of Contents

List of Figures

List of Tables

List of Abbreviations

CSPR	:	Cable Suspended parallel Robot
CDPR	:	Cable Driven Parallel Robot
DBCDPR	:	Dual Base Cable Driven Parallel Robot
DOF	:	Degrees of Freedom
EE	:	End Effector
FAD	:	Feasible Acceleration Diagram

1. INTRODUCTION

A Cable suspended parallel robot (CSPRs) is a type of cable driven parallel manipulator (CDPRs) that has recently become popular for large workspace operations. CDPRs generally consist of two fixed bases, one on top of the workspace and the other on its bottom (See Figure 1.1) making the dual base CDPRs (DBCDPR). A CSPR only has a single fixed base on top of the workspace (See figure 1.2). This enables CSPRs to maneuver in extended workspaces, where motions of DBCDPR are hindered by cables attached to its bottom platform. However, in contrast to DBCDPRs, CSPRs generally use gravity to maintain the cables in tension. Similar to DBCDPRs, CSPRs also use a mobile platform (referred to as the End-Effector, EE in this thesis) connected in parallel to the base through flexible cables and motorized winches. The cables are extended or retracted by means of the winches to control the motion of EE. The advantages of CDPRs (both DBCDPRs and CSPRs) over common parallel robot architectures are;

(i.) The heavy components (Base platform, winches) of a CDPR lies stationary which results in low inertial properties, high payload to weight ratios, and fast motions.

(ii.) Possibility to work in very large workspaces as cables can be unwound over great lengths.

(iii.) Easy transportability and re-configurability.

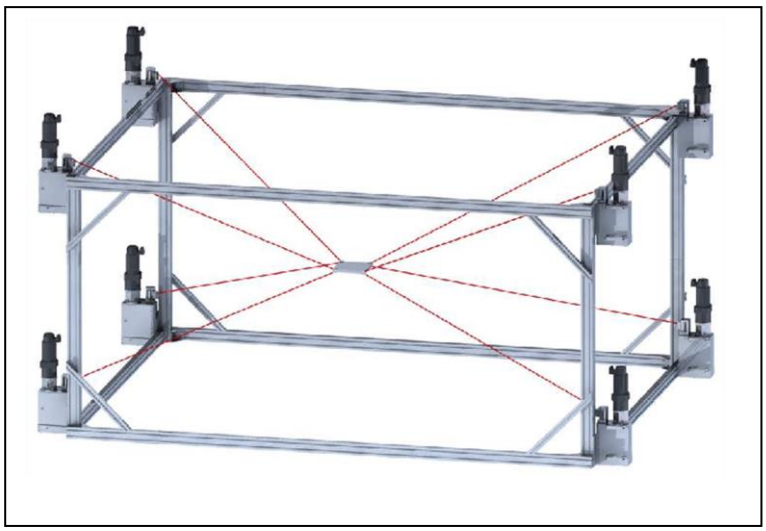

Figure 1.1: Dual Base CDPR
Source: www.researchgate.net

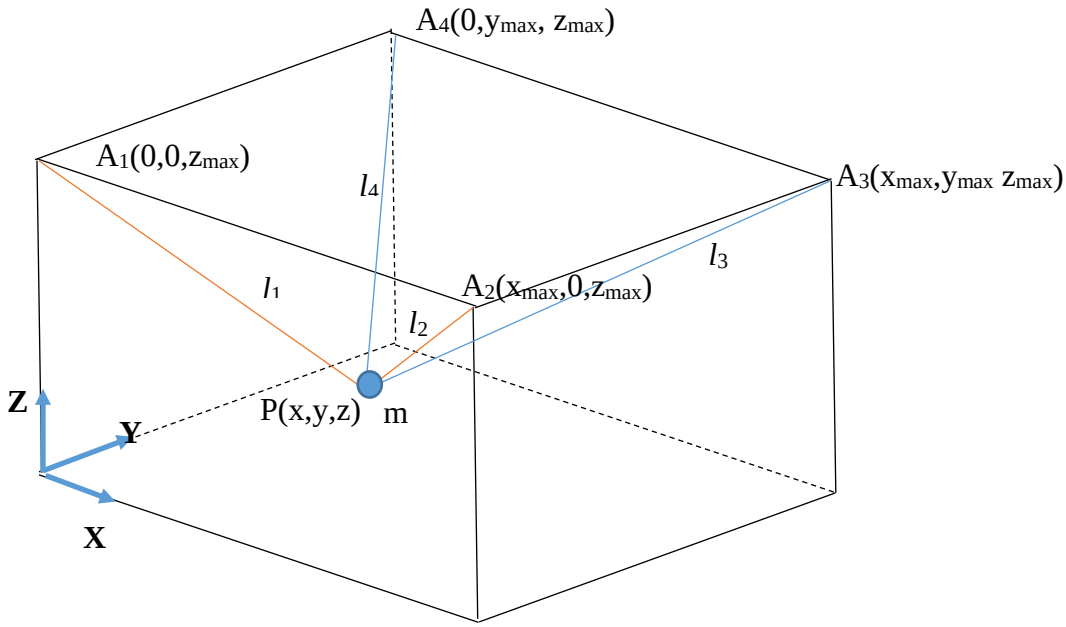

Figure 1.2: Cable Suspended Parallel Robot: 3-DoF: 4Cable Configuration

Although CSPRs possess extended workspace capabilities over DBCDPRs, they also possess the disadvantage of limited dynamics in motion due to combination of two factors, namely:

(i.) Inability of the cables to work in compression (cables can only pull, and cannot push)

(ii.) Unlike in DBCDPRs the maximum force feasible in downward direction is the constant force of gravity.

1.1 Literature review

Limitation of dynamics works as a considerable challenge in designing feasible trajectories for CSPRs. Indeterminable cable tensions work as an additional hindrance in designing feasible trajectories particularly for redundantly actuated CSPRs (described in section 1.2 of this thesis). Consequently, in most cases found in literature or implemented in practice CSPRs are assumed to work in static or quasi-static

conditions. Most of the work reported in the literature does not address the dynamics of cable-suspended robots and uses techniques based on static equilibrium to solve control and design problems. For example, under the quasi-static assumption, the workspace of a cable-suspended robot is limited to configurations (poses) for which static equilibrium can be reached while maintaining all cables under tension [1] .

Dynamic trajectory planning is addressed in several research papers for fully actuated (Non-redundant) CSPRs for,

(i.) 2 Degrees of Freedom (DOF) Planer ([1])

(ii.) 3DOF planar (Motion in vertical plane considered with moments) ([2], [10], [13]), and

(iii.) 3DOF (spatial - Point mass EEs) ([3], [4], [5])

Several research papers have addressed the issue of determining cable tensions in redundant CSPRs by introducing certain techniques ([6], [7], [11], [8], [12]). However, all these makes certain assumptions while determining the cable tensions. For examples [6] assumes the variance between cable tensions to be a minimum. [7], [11], [12] assume static/quasi-static equilibrium. This issue, together with disadvantages of CSPRs discussed above acts as a hindrance to find suitable dynamic trajectories for CSPRs. This demands development of techniques that by-passes the cable tension determination while ensuring positive tension in cables throughout the trajectory.

1.2 Existing system and problem statement

Accurate determination of many factors affects the precise calculation of cable tensions. In practice, cables with low to very low elastic properties are used for the operations. Due to this even a small error in determining the cable lengths can greatly affect the calculation of cable tensions. Among other factors that lead to errors in determination of cable tensions sagging of cables during low payload ([15]) is significant and due to this the cable system will have time delays while attaining their equilibrium strains in dynamic operations.

In fully actuated 3DOF point mass - spatial robots, EE is controlled by three winches located in three points in space, generally at the same height. In this case, the footprint of workspace of EE is limited to the horizontal plane projected to ground by the triangle connecting three winches. In practice, most spatial operations such as picking and placing objects (For examples in warehouses, fuel-yards, etc.) demand a rectangular footprint. In this case, when the 4th actuator is added a point mass EE will be redundantly actuated. Consider the schematic of a 3DOF (spatial) 4-cable configuration in figure 1.2. The workspace is bounded by the vertical projection of the rectangle $A_1A_2A_3A_4$ on a horizontal plane vertically down to its rectangular footprint on another horizontal plane at a distance of z_{max}. EE (at variable position B) is controlled by extracting and retracting cables BA_1, BA_2, BA_3 and BA_4 by winches, each at A_1, A_2, A_3, and A_4. Lengths of the cable are l_1 , l_2 , l_3 and l_4 and vectors from EE to winches are L_1, L_2, L_3 and L_4 respectively. Position vector of EE with reference to fixed origin is $(x, y, z)^T$ where x, y and z are the distances from origin to EE in respective directions X, Y and Z. If the magnitudes of tensions in cables are T_1, T_2, T_3 andT_4, equation of motion ($F=ma$) of EE can be written as:

$\sum_{i=1}^{4} \frac{L_i}{l_i} T_i - g = m(\ddot{x} \quad \ddot{y} \quad \ddot{z})^T$where $(\ddot{x} \quad \ddot{y} \quad \ddot{z})^T$ is the acceleration of EE.

$$\begin{pmatrix} -x \\ -y \\ z_{max} - z \end{pmatrix} \frac{T_1}{l_1} + \begin{pmatrix} x_{max} - x \\ -y \\ z_{max} - z \end{pmatrix} \frac{T_2}{l_2} + \begin{pmatrix} x_{max} - x \\ y_{max} - y \\ z_{max} - z \end{pmatrix} \frac{T_3}{l_3} + \begin{pmatrix} -x \\ y_{max} - y \\ z_{max} - z \end{pmatrix} \frac{T_4}{l_4} - g = m \begin{pmatrix} \ddot{x} \\ \ddot{y} \\ \ddot{z} \end{pmatrix} \quad (1)$$

Where, $l_1 = \frac{1}{\sqrt{(-x)^2+(-y)^2+(z_{max}-z)^2}}$;

$l_2 = \frac{1}{\sqrt{(x_{max}-x)^2+(-y)^2+(z_{max}-z)^2}}$;

$l_3 = \frac{1}{\sqrt{(x_{max}-x)^2+(y_{max}-y)^2+(z_{max}-z)^2}}$, and

$l_4 = \frac{1}{\sqrt{(-x)^2+(y_{max}-y)^2+(z_{max}-z)^2}}$.

Three equations can be obtained by separating out the vector elements of equation (1) into their respective directions. Yet, there are four unknown magnitudes of cable

tensions. This makes the tensions of cables indeterminate although all the accelerations and positions are known. This makes the design of feasible dynamics for the motion a challenge.

1.3 Objective

Objective of this research thesis is to introduce and analyze an analytical model to circumvent the cable tension determination problem using a concept termed as 'Feasible Acceleration Diagram' and design a time optimized point – to –point straight line trajectory with smooth dynamics for redundantly actuated 2DOF (planer) and 3DOF (spatial) CSPRs while ensuring positive cable tensions.

Organization of the remaining chapters of this thesis are as follows.

Chapter-2: The concept of Feasible Acceleration Diagrams (FAD) will be introduced. Conditions will be developed for feasible accelerations.

Chapter-3: A suitable model will be developed for point – to – point, straight line trajectory with smooth dynamics. This model will be applied in conditions developed in Chapter-2.

Chapter-4: An experiment will be carried out to verify the theories developed and the results will be simulated. A numerical method will be used to verify the validity of optimal duration time.

Chapter-5: Discusses and summarizes the results. Areas of future works are discussed.

2. FEASIBLE ACCELERATIONS DIAGRAM (FAD)

In this section first, the concept of Feasible Acceleration Diagrams (FAD) will be introduced using a 2DOF, 2-Cable configuration. This section will then illustrate the FAD model with respect to 2 DOF – 3 cable and 3DOF (spatial) – 4 cable configurations.

2.1 Feasible acceleration diagram for 2 DOF (planar), 2-Cable configuration

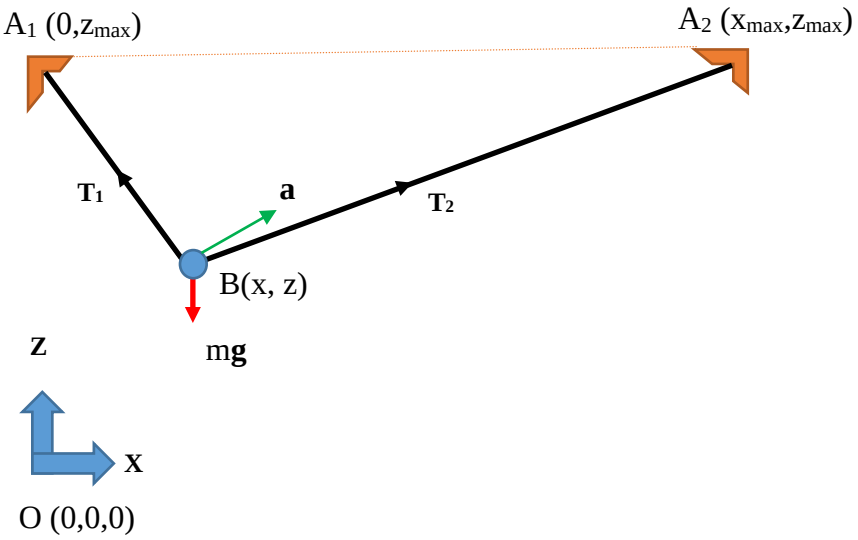

Figure 2.1: 2DOF (Planar), 2Cable configuration

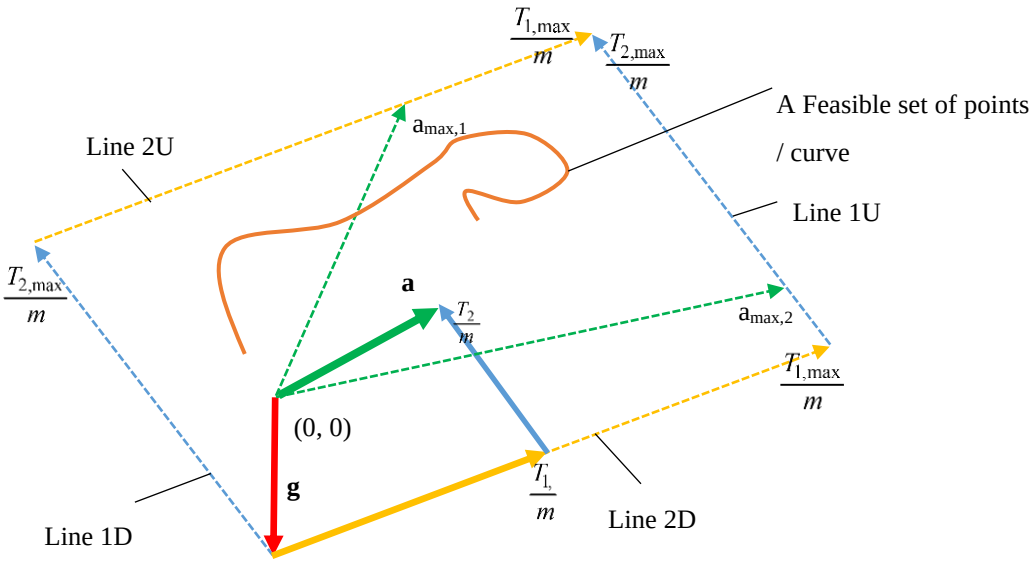

Figure 2.2: 2DOF, 2Cable Feasible Acceleration Diagram

A theory comparable to below described has been used in [9], [14] while constructing Wrench feasible Workspaces. Consider the 2 DOF - 2 Cable configuration shown in Figure 2.1. This shows a point mass load (EE) controlled by two cables actuated by two spools fixed to a stationary base in a horizontal line. The position of EE with reference to the fixed reference frame X-Z shown is *(x, z)*. Positions of spools: A_1 and A_2 from where the cables 1 and 2 are extending, are given by (0, z_{max}) and (x_{max}, z_{max}) respectively. Horizontal line A_1A_2 and vertical line A_1O are two adjacent sides of the rectangular workspace of EE, whereas OA_2 is its diagonal. Mass of the load (EE) is m, and the gravitational force is mg. At time = t, tensions of cables attached to EE are T_1 and T_2 as shown. EE is experiencing an acceleration, 'a' in the direction shown due to the forces. Note that any force (F) acting on EE contributes a vector $\frac{F}{m}$ to build up the resultant acceleration vector a. Thus, the vectors $\frac{T_1}{m}$, $\frac{T_2}{m}$ and g ($= \frac{mg}{m}$) are the components in acceleration of EE contributed by two cable forces and the gravitational force respectively.

Figure 2.2 shows the corresponding vector diagram of these acceleration vectors, in thick colored lines. The diagram also shows the maximum allowable acceleration vectors $\frac{T_{1,max}}{m}$ and $\frac{T_{2,max}}{m}$ the cables are capable of providing due to limitations in safe cable tensions and/or torque limits of the motors. It should be noted that $\frac{T_1}{m}$ and $\frac{T_2}{m}$ shall essentially lie within $\frac{T_{1,max}}{m}$ and $\frac{T_{2,max}}{m}$ respectively. g is fixed. It should be noted that the boundary of set of feasible accelerations are the edges of the parallelogram generated by $\frac{T_{1,max}}{m}$ and $\frac{T_{2,max}}{m}$. In other words, if the acceleration vector lies inside this parallelogram, there exists a combination of feasible cable tensions that provides this acceleration. The position vector of any point inside the diagram relative to point (0, 0) shows a feasible resultant acceleration. Two sample maximum accelerations are shown in the diagram as $a_{max,1}$ and $a_{max,2}$ to illustrate this. Diagram in figure 2.2 will here in after be referred to as Feasible Accelerations Diagram (FAD). Since the position of EE is identified in relation to the fixed X-Z reference, geometry of FAD can be known with respect to x, y, x_{max}, z_{max}, and magnitudes of $\frac{T_{1,max}}{m}$ and $\frac{T_{2,max}}{m}$.

Generally, the magnitudes of both $T_{1,\max}$ and $T_{2,\max}$ can be taken as a single value T_{max} since the allowable tensions in cables do not change from cable to cable. In Cartesian coordinates, each point in the plane of the diagram refers to a specific $(\frac{d^2x}{dt^2}, \frac{d^2z}{dt^2})$. This will herein after be designated as $(\ddot{x}, \ddot{z})$. Thus, all the boundary lines limiting the feasible accelerations can be defined as a linear relationship between $\ddot{x}\ and\ \ddot{z}$ provided the values of x, y, x_{max}, z_{max} and magnitudes of $\frac{T_{1,max}}{m}$ and $\frac{T_{2,max}}{m}$. Throughout any feasible trajectory, all the $(\ddot{x}, \ddot{z})$ points corresponding to accelerations should lie inside the FAD. Provided the EE will not move vertically beyond the horizontal line connecting the spools, this is the necessary and adequate condition for a feasible trajectory. A sample feasible curve of $(\ddot{x}, \ddot{z})$. is also shown in figure 2.2.

General inequality corresponding to boundary lines 1D and 2D is given below. Deduction of these inequalities are shown in Appendix A.

$$\ddot{z} = \frac{(z_{max}-z)}{(p_i-x)}\ddot{x} - g \qquad (2)$$

where $p_1 = 0$; $p_2 = x_{max}$; and i indicates the direction of each line in FAD which corresponds to directions of cables.

Allowable tensions in cables can be designed in very high values, such that the values of $\frac{T_{1,max}}{m}$ and $\frac{T_{2,max}}{m}$. are very large compared to gravitational acceleration, g. Therefore, the lower tension limits will dominate the feasibility of trajectories. Due to this, and since the scope of this thesis is limited to ensuring 'positive cable tensions' throughout the trajectories, equations of lines corresponding to boundaries 1U and 2U will not be analyzed herein.

2.2 Feasible accelerations diagram for 2DOF (planar), 3-Cable configuration

When a redundant 3rd cable is added into the 2-DoF (planar) cable system as (see figure 2.3) it will modify the FAD as shown in figure 2.4. The configuration is similar to that in section 2.1 except the addition of another cable to EE from a controlling spool which lies between A_1 and A_2.

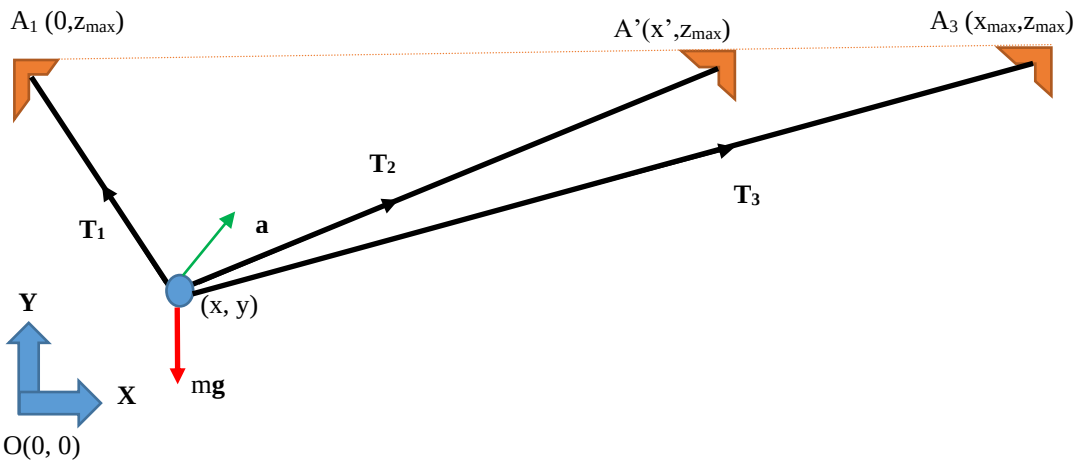

Figure 2.3: 2DOF, 3-Cable Configuration

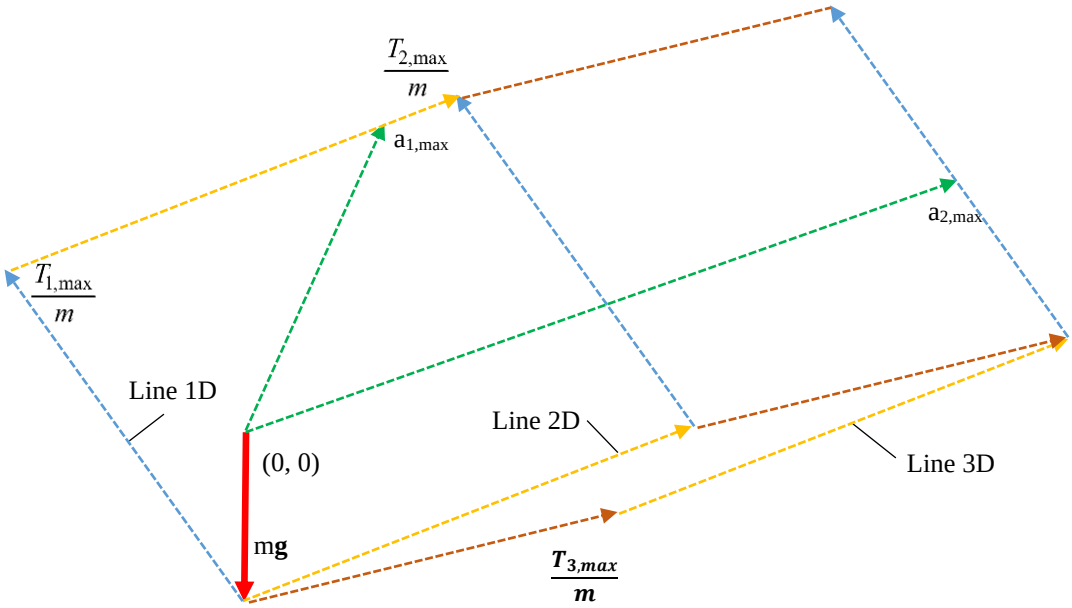

Figure 2.4: 2DOF, 3 Cable Feasible Acceleration Diagram

In this case, the FAD becomes a hexagon of three parallel couples of edges on opposite sides. It should be noted that if the acceleration vector lies inside the upper angle generated by $\frac{T_{1,max}}{m}$ and $\frac{T_{3,max}}{m}$ at all times during a trajectory, there exists a combination of non-negative cable tensions which can provide this acceleration. Thus, the accelerations are feasible, assuming the upper tension limits are significantly high. In case the acceleration is completely inside the angle {i.e. $(\ddot{x}, \ddot{z})$ is inside the angle and does not lie on its edges} there are infinite number of such combinations.

Conversely, if $(\ddot{x}, \ddot{z})$. lies outside the angle such accelerations are not feasible. Therefore, $(\ddot{x}, \ddot{z})$. being inside the edges of this angle is the necessary and sufficient condition for feasible accelerations. Inequalities corresponding to these limits have the same form as (1), where $p_1 = 0$, $p_2 = x'$ and $p_3 = x_{max}$. Note that, in this setting it is suffice to maintain only the inequalities imposed by lines 1D and 3D at all times.

2.3 Feasible acceleration diagram for 3-DOF (spatial), 3-Cable configuration

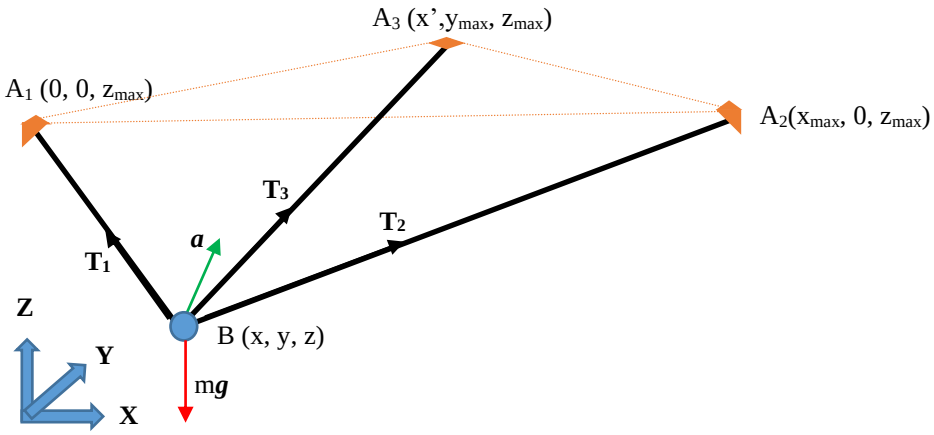

Figure 2.5: 3DOF (Spatial), 3-Cable configuration

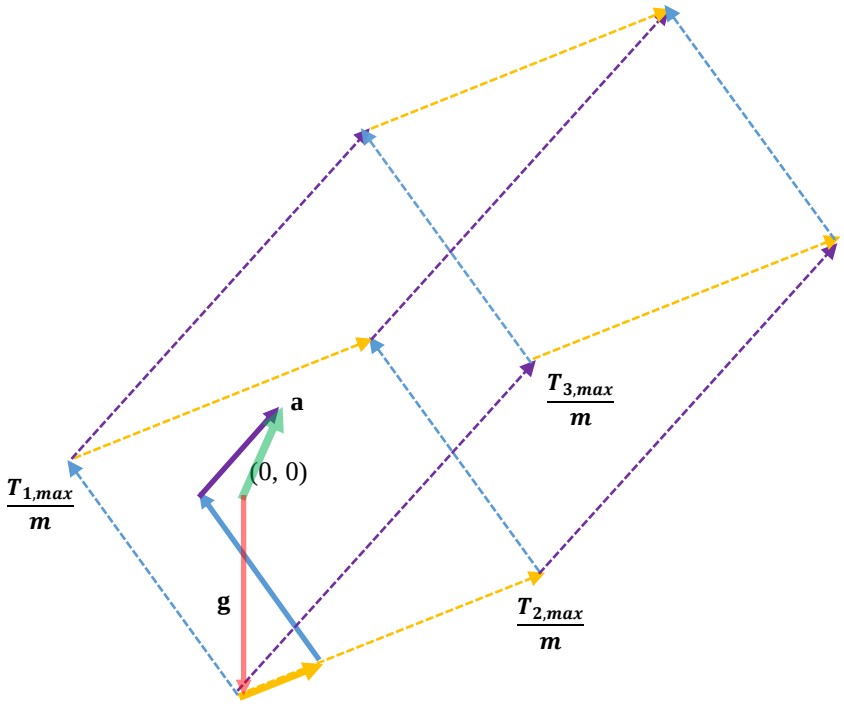

Figure 2.6: 3DOF, 3-Cable Feasible Acceleration Diagram

Consider the 3 DOF (Spatial), 3Cable configuration shown in Figure 2.5. This figure shows a point mass load (EE) at variable point B controlled by three cables actuated by three spools each fixed at corners A_1, A_2 and A_3 of a stationary triangular base. This base lies on a horizontal plane. The workspace is limited to the trapezium generated by projecting triangle $A_1A_2A_3$ vertically down to its triangular footprint on another horizontal plane at a distance z_{max}. Origin of the fixed reference frame is on this plane vertically below A_1. X axis is parallel to A_1A_2. Z-axis is along OA_1. Position of EE with reference to the fixed reference frame is (x. y, z). Positions of A_1, A_2 and A_3 are given by (0, 0, z_{max}), (x_{max}, 0, z_{max}) and (x', y_{max}, z_{max}) respectively. Mass of the load (EE) is m. Gravitational force is mg. At time = t, tensions of cables attached to EE are T_1, T_2 and T_3 as shown. EE is experiencing an acceleration, a in the direction shown due to the forces.

FAD of above configuration is a parallelepiped, which is a three-dimensional figure. This is shown in figure 2.6. Maximum acceleration components the cables are capable of providing are shown in dotted lines. Respective acceleration component vectors are shown in thick colored lines. In this case, the boundary of set of feasible accelerations, are the faces of the parallelepiped generated by $\frac{T_{1,max}}{m}$, $\frac{T_{2,max}}{m}$ and $\frac{T_{3,max}}{m}$ vectors. Position vector of any point inside the parallelepiped relative to point (0, 0, 0) shows a feasible resultant acceleration. As the position of EE is identified in relation to the fixed X-Y-Z reference frame, geometry FAD will be known with respect to x, y, z, x_{max}, y_{max}, z_{max} and the magnitudes of $\frac{T_{1,max}}{m}$, $\frac{T_{2,max}}{m}$ and $\frac{T_{3,max}}{m}$. Each point in the diagram refers to a specific $(\frac{d^2x}{dt^2}, \frac{d^2y}{dt^2}, \frac{d^2z}{dt^2})$, which will herein after be referred to as $(\ddot{x},\ \ddot{y},\ \ddot{z})$. Thus, all the boundary lines limiting the feasible accelerations can be defined as a linear relationship between $\ddot{x},\ \ddot{y}$ and $\ddot{z}$ provided the values of x, y, u, v, and magnitudes of $\frac{T_{1,max}}{m}$, $\frac{T_{2,max}}{m}$ and $\frac{T_{3,max}}{m}$. Inequalities for this 3-DOF - 3 cable configuration will not be developed since the purpose of this thesis is to analyze 4-cable scenario for 3DOF spatial scenario, which will be discussed next.

2.4 Feasible acceleration diagram for 3-DOF (spatial), 4-Cable configuration

Consider the 3 DOF (Spatial), 4Cable configuration shown in Figure 2.7. This shows a point mass load (EE) in variable point B controlled by four cables actuated by four spools each fixed at corners A_1, A_2, A_3 and A_4 of a stationary rectangular base in a horizontal plane.

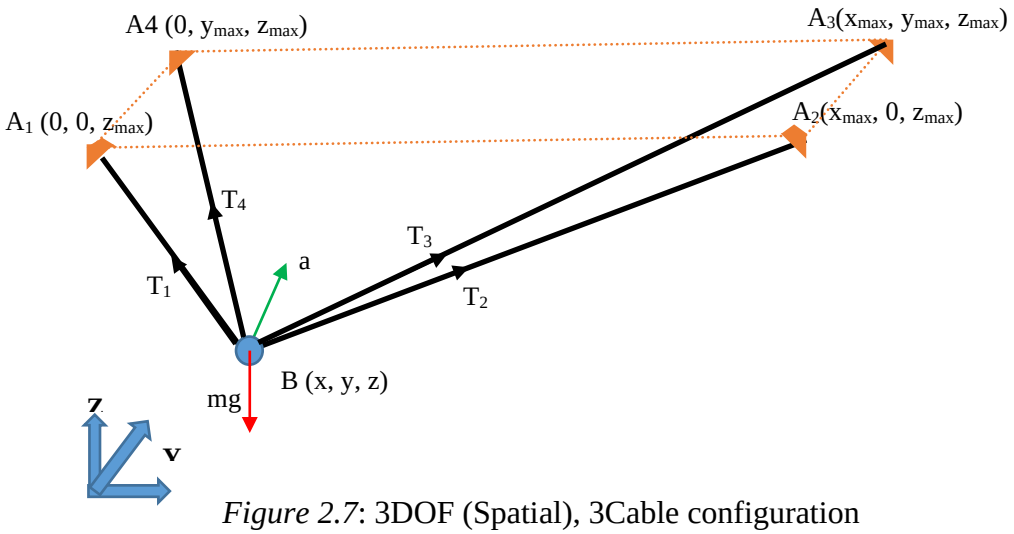

Figure 2.7: 3DOF (Spatial), 3Cable configuration

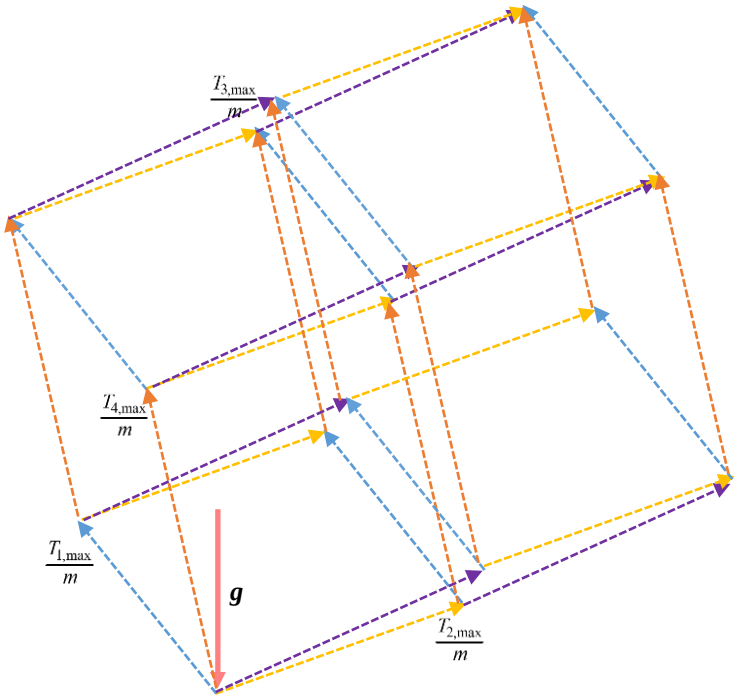

Figure 2.8: 3DOF, 4-Cable Feasible Acceleration Diagram

The workspace is limited to the cuboid generated by projecting $A_1A_2A_3A_4$ vertically down to its rectangular footprint on another horizontal plane at a distance z_{max}. Origin of the fixed reference frame lies on this plane vertically below A_1. X-axis is parallel to A_1A_2, Z-axis is along OA_1. The position of EE with reference to the fixed reference frame is given by (x. y, z). Positions of are A_1, A_2, A_3 and A_4 are given by (0, 0, z_{max}), (x_{max}, 0, z_{max}), (x_{max}, y_{max}, z_{max}) and (0, y_{max}, z_{max}) respectively. Mass of the load (EE) is m, and the gravitational force is mg. At time = t, tensions of cables attached to EE are T_1, T_2 , T_3 and T_4. EE is experiencing an acceleration a in the direction shown due to the forces.

The FAD in this configuration is given in figure 2.8. This figure shall be constructed by adding 8 additional edges in FAD of 3DoF, 3-cable case (see Figure 2.6) starting from each of its vertices. The resulting solid is a polyhedron with 12 faces. This figure is called a dodecahedron. Each face of this polyhedron is a parallelogram. The number of surfaces can be obtained by calculating the permutation: ${}_{(Number\ of\ tension\ vectors)}2p$. Lower bounds of this FAD resemble an inverted pyramid having edges $\frac{T_{1,max}}{m}$, $\frac{T_{2,max}}{m}$, $\frac{T_{3,max}}{m}$ and $\frac{T_{4,max}}{m}$.

In this case, If the acceleration vector lies inside the said inverted pyramid (whose edges may extend indefinitely), there exists a combination of non-negative cable tensions that can provide this acceleration. Further, if the acceleration vector is completely inside the inverted pyramid {i.e. $(\ddot{x}, \ddot{y}, \ddot{z})$ lie within the surfaces but not on any surface, there are infinite number of such combinations. Conversely, if the acceleration vector breaches these boundary limits at least one tension shall become negative to provide that acceleration. Therefore, $(\ddot{x}, \ddot{y}, \ddot{z})$ being inside the edges of the said inverted pyramid at all times during the trajectory is the necessary and sufficient condition for feasible accelerations.

Inequalities corresponding to the required conditions are given below. Deduction of corresponding equations are given in Part-2 of Appendix A.

$$\ddot{z} \geq (\frac{z_{max}-z}{-y})\ddot{y} - g \qquad (3)$$

$$\ddot{z} \geq \left(\frac{z_{max}-z}{x_{max}-x}\right)\ddot{x} - g \quad (4)$$

$$\ddot{z} \geq \left(\frac{z_{max}-z}{y_{max}-y}\right)\ddot{y} - g \quad (5)$$

$$\ddot{z} \geq \left(\frac{z_{max}-z}{-x}\right)\ddot{x} - g \quad (6)$$

Note that, in order to remain within the lower bounds of FAD (inside the 'inverted pyramid'), all inequalities imposed in (3) – (6) shall be satisfied at all times.

3. FORMATION OF A MODEL FOR POINT TO POINT STRAIGHT LINE TRAJECTORY WITH SMOOTH DYNAMICS

In this section, a suitable kinematical model will be developed for point – to – point, straight line trajectory with smooth dynamics. This will then be applied in the inequalities developed in section 2 to use as a basis for time optimization.

3.1 Basic requirements

It shall be noted that a point to point straight line trajectory used for pick and place type of operations shall have following characteristics

1. Dynamics of the trajectory shall be smooth. In other words, the 3rd derivative of displacement (jerk) shall have a finite value at all times. For this, the acceleration of EE as well as the cables shall be continuous.
2. Both at the start and the end of the traverse, accelerations and velocities shall be zero. Therefore,
   $\ddot{X}(0) = 0\,; \dot{X}(0) = 0\,; \ddot{X}(T) = 0\,; \dot{X}(T) = 0$, where X(t) is the position vector $(x, y, z)^T$ of EE at time = t.
3. In order to remain in a straight-line, magnitudes of velocity components parallel to each reference axis X, Y and Z should be same at any given time. Thus, $\dot{x}(t) = \dot{y}(t) = \dot{z}(t)$

3.2 Formation of kinematics

To satisfy above basic requirements and to have a provision to optimize the duration of trajectory a scenario where EE is traversing in a straight line from point B_0 to point B_1 is now discussed. In order to satisfy these conditions stipulated, the kinematics of motion is modelled as;

$$X(t) = X_0 + (X_1 - X_0)s(t) \qquad (7)$$

where $s(\ddot{t})$ is given by table 3.1, for $0 \leq t \leq T$and

for 2DoF (Planar) case:

X_0: Position vector of the initial position of EE, B_0: $[x_0 \quad z_0]^T$

X_1: Position vector of the final position of EE, B_1: $[x_1 \quad z_1]^T$, and

for 3DoF (Spatial) case:

X_0: Position vector of the initial position of EE, B_0: $[x_0 \quad y_0 \quad z_0]^T$

X_1: Position vector of the final position of EE, B_1: $[x_1 \quad y_1 \quad z_1]^T$, and

Table 3.1: $\ddot{s}(t)$ Values of Displacement function

Range of time	$0 \le t < \frac{p}{2}$	$\frac{p}{2} \le t < p$	$p \le t < \frac{T+p}{2}$	$p \le t < T$
$\ddot{s}(t)$	$\frac{8t}{p^2T}$	$\frac{8(p-t)}{p^2T}$	$-\frac{8(t-p)}{T(T-p)^2}$	$-\frac{8(T-t)}{T(T-p)^2}$

Variable *p* is introduced to fine tune the optimization. The use of this variable will be justified while optimizing the duration in chapter 4. Graph in figure 3.1 shows the behavior of $\ddot{s}(t)$. Values on table 3.1 have been calculated using this graph. Maximum acceleration, has been set to value $\frac{4}{pT}$ by reverse calculating it to ensure *s(T)* = 1. This model will be referred to as the S-Model hereafter.

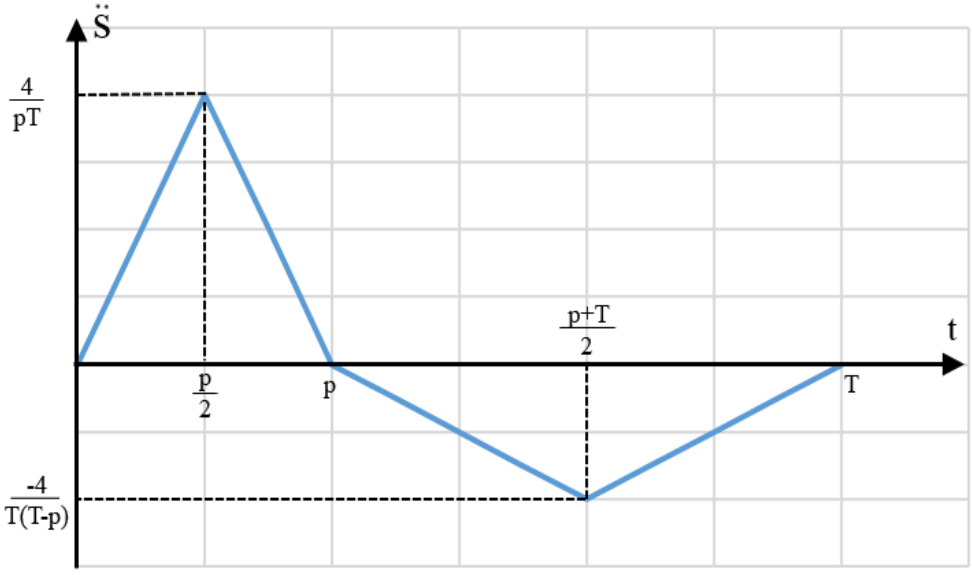

Figure 3.1: Behavior modelled for $\ddot{s}(t)$

By differentiating (7),

$\dot{X}(t) = (X_1 - X_0)\dot{s}(t)$, and (8)

$\ddot{X}(t) = (X_1 - X_0)\ddot{s}(t)$ (9)

MATLAB MuPAD is used to calculate the functions: $\dot{s}(t)$ and $s(t)$. These functions, as well as Functions obtained for $\ddot{s}(t), \dot{s}(t)$, and $s(t)$ are given in table 3.2.

Table 3.2: Behavior of $\ddot{s}(t), \dot{s}(t)$, and $s(t)$

	$\ddot{s}(t)$	$\dot{s}(t)$	$s(t)$
$0 \le t < \frac{p}{2}$	$\frac{8\,t}{T\,p^2}$	$\frac{4\,t^2}{T\,p^2}$	$\frac{4\,t^3}{3\,T\,p^2}$
$\frac{p}{2} \le t < p$	$\frac{8\,(p-t)}{T\,p^2}$	$\frac{1}{T} - \frac{(3\,p-2\,t)\,(p-2\,t)}{T\,p^2}$	$\frac{p}{6\,T} + \frac{p^3 - 12\,p^2\,t + 24\,p\,t^2 - 8\,t^3}{6\,T\,p^2}$
$p \le t < \frac{T+p}{2}$	$\frac{8\,(p-t)}{T\,(T-p)^2}$	$\frac{2}{T} - \frac{4\,(p-t)^2}{T\,(T-p)^2}$	$\frac{p}{T} - \frac{2\,(p-t)\,(3\,T^2 - 6\,T\,p + p^2 + 4\,p\,t - 2\,t^2)}{3\,T\,(T-p)^2}$
$p \le t < T$	$-\frac{8\,(T-t)}{T\,(T-p)^2}$	$\frac{4\,T^2 - 8\,T\,t + 4\,t^2}{T\,(T-p)^2}$	$\frac{-T^3 - 6\,T^2\,p + 12\,T^2\,t + 3\,T\,p^2 - 12\,T\,t^2 + 4\,t^3}{3\,T\,(T-p)^2}$

Values of $\ddot{s}(t), \dot{s}(t)$ and $s(t)$ for changing points of acceleration gradient are given in Table 3.3.

Table 3.3: Values of $\ddot{s}(t), \dot{s}(t)$ and $s(t)$ at changing points of acceleration gradient

	$\ddot{s}(t)$	$\dot{s}(t)$	$s(t)$
$t = 0$	0	0	0
$t = \frac{p}{2}$	$\frac{4}{T\,p}$	$\frac{1}{T}$	$\frac{p}{6\,T}$
$t = p$	0	$\frac{2}{T}$	$\frac{p}{T}$
$t = \frac{T+p}{2}$	$-\frac{4}{T\,(T-p)}$	$\frac{1}{T}$	$\frac{p}{6\,T} + \frac{5}{6}$
$t = T$	0	0	1

Behavior of $\ddot{s}(t), \dot{s}(t)$ and $s(t)$ for p = 2.5, and T = 10 are given in figures 3.2 (a), 3.2 (b) and 3.2 (c) respectively.

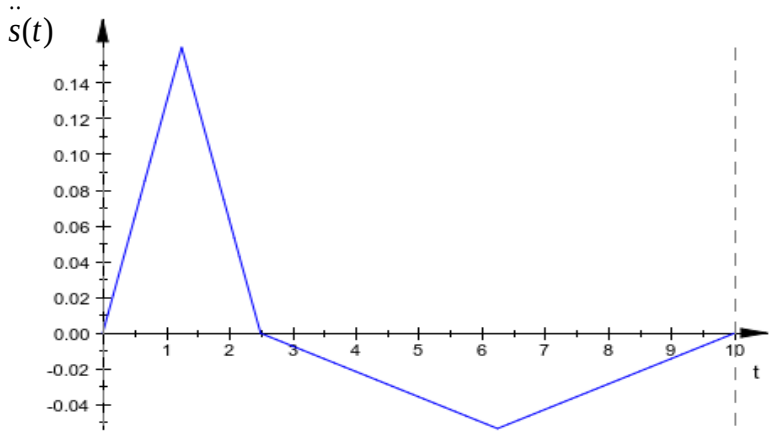

Figure 3.2 (a): Behavior of $\ddot{s}(t)$ at sample values

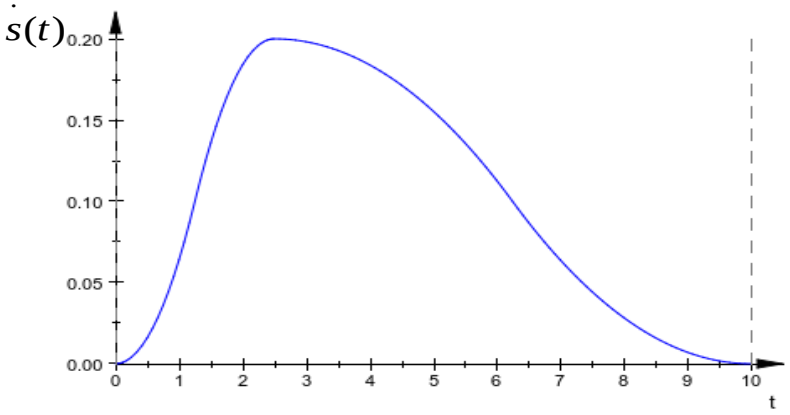

Figure 3.2 (b.) :Behavior of $\dot{s}(t)$ at sample values

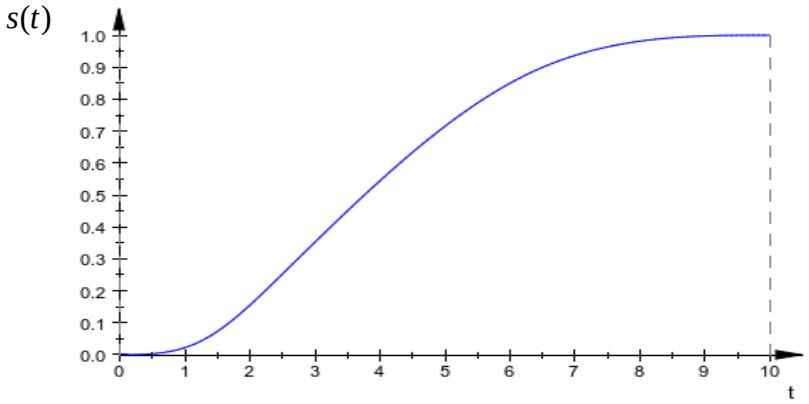

Figure 3.2 (c.): Behavior of acceleration $s(t)$ at sample values

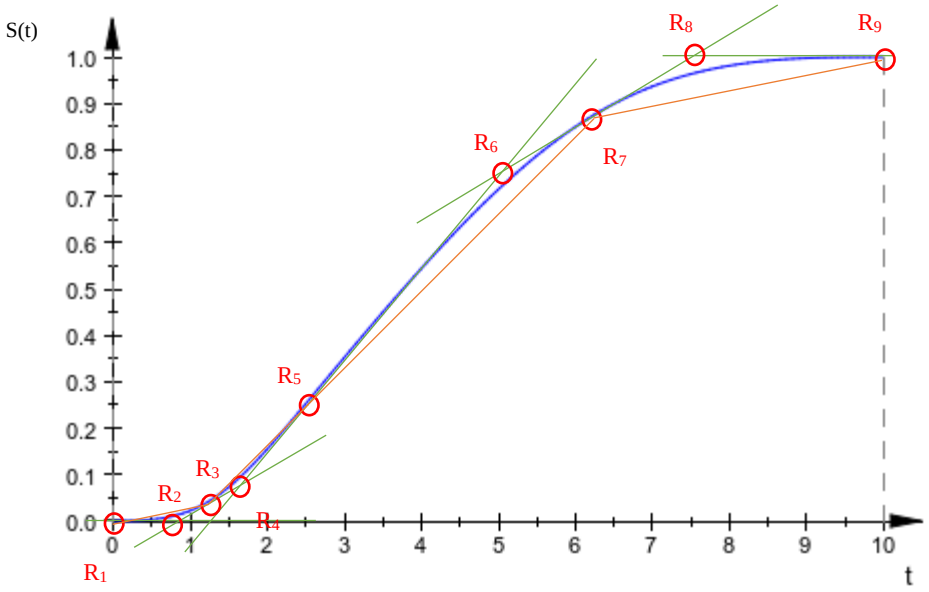

Figure 3.3: Illustration of P-points

3.3 Formation of time optimization strategy

The sample of s(t) curve obtained above in figure 3.3 will be used to illustrate the following:

Consider the tangents of the function $s(t)$ drawn at points: R_1, R_3, R_5, R_7 and R_9 for any $s(t)$ vs. t curve. These points shall be so selected such that the tangents to curve

Table 3.4: Values of t and $s(t)$ at changing points of acceleration gradient (Odd 'R'-points)

Point	**t**	**s**
R_1	0	$\frac{p}{6T}$
R_3	$\frac{4}{Tp}$	$\frac{p}{6T}$
R_5	p	$\frac{p}{T}$
R_7	$\frac{T+p}{2}$	$\frac{p}{6T}+\frac{5}{6}$
R_9	T	1

toward either direction (t+ or t-) from these points are either continuously increasing up to the next point, or continuously decreasing. Since the turning points of $\ddot{s}(t)$ are ideal points satisfying this requirement, they have been selected as these points. Therefore, R_2, R_4, R_6, and R_8 are the points where each above tangent intersects the subsequent tangent. Since $s(t)$ curve is continuous, and tangents are selected in the manner described above, it is clear that curve *s(t)* always lies inside the triangles (R_1, R_2, R_3), (R_3, R_4, R_5), (R_5, R_6, R_7) and (R_7, R_8, R_9). Since all $s(t)$ values and the respective gradients of tangents $\{\dot{s}(t)\}$ of corresponding points R_1, R_3, R_5, R_7, R_9 are already known, points R_2, R_4, R_6, R_8 can be found. Since t_i (i=1..9) are now known, corresponding values of $\ddot{s}(t)$ (i=1..9) can also be calculated.

Table 3.5: Q-points

$\boldsymbol{i}$	$\boldsymbol{t}$	$\boldsymbol{s(t)}$	$\boldsymbol{\ddot{s}(t)}$
1	0	0	0
2	$\frac{p}{3}$	0	$\frac{8}{3Tp}$
3	$\frac{p}{2}$	$\frac{p}{6T}$	$\frac{4}{Tp}$
4	$\frac{2p}{3}$	$\frac{p}{3T}$	$\frac{8}{3Tp}$
5	p	$\frac{p}{T}$	0
6	$\frac{T+2p}{3}$	$\frac{2T+p}{3T}$	$-\frac{8}{3T(T-p)}$
7	$\frac{T+p}{2}$	$\frac{p}{6T}+\frac{5}{6}$	$-\frac{4}{T(T-p)}$
8	$\frac{2T+p}{3}$	1	$-\frac{8}{3T(T-p)}$
9	T	1	0

It can be proven that since $\ddot{s}(t)$ is piecewise linear in t between odd points R_i (i = 1, 3, 5, 7, 9) the curve drawn $\ddot{s}(t)$ vs. $s(t)$ shall also lie inside the respective triangles (Q_1, Q_2, Q_3), (Q_3, Q_4, Q_5), (Q_5, Q_6, Q_7) and (Q_7, Q_8, Q_9) at all times, where Q_i = $\{s(t), \ddot{s}(t)\}$, i=1..9. Proof of this is given in Appendix B. Values of all Q points, together with corresponding t_i values are given in table 3.5.

Figure 3.4 shows the plot of $\ddot{s}(t)$ vs. $s(t)$ plot together with relevant triangles for p=2.5; T=10. This figure will be referred to illustrate the following:

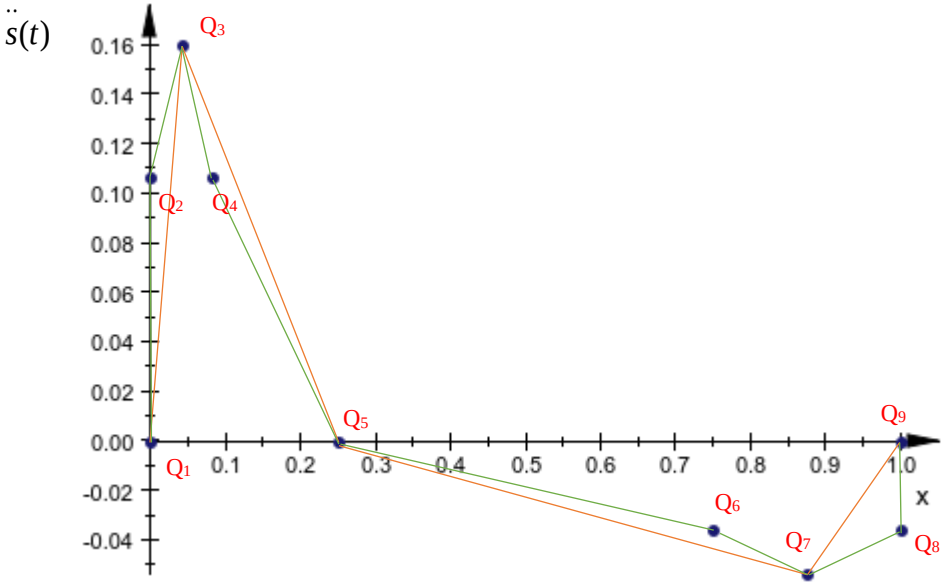

Figure 3.4: Illustration of Q-points

With regard to the values of the points, following gradients could be found:

(i.) Gradient between Q_3 and Q_4 is $-\frac{24}{5p^2}$, whereas gradient between Q_3 and Q_5 is $-\frac{4}{p^2}$. Therefore |gradient (Q_3 and Q_5)| ≤ |gradient (Q_3 and Q_4)|, and both gradients are negative.

(ii.) Gradient between Q_5 and Q_6 is $-\frac{4}{(T-p)^2}$, whereas gradient between Q_5 and Q_7 is $-\frac{24}{5(T-p)^2}$. Therefore |gradient (Q_3 and Q_5)| ≤ |gradient (Q_3 and Q_4)|, and both gradients are negative.

(iii.) Gradient between Q_1 and $Q_5 = 0$, whereas gradient between Q_1 and Q_7 is $-\frac{24}{5(5T+p)(T-P)}$.

(iv.) Gradient between Q_5 and Q_9 $=-\frac{24}{(6T-p)P}$, whereas gradient between Q_5 and Q_9 is 0.

Therefore, in case the curve $\ddot{s}(t)$ vs. $s(t)$ shall be conditioned (tuned by varying p and T values) such that, it shall not lie outside a given straight line on the above diagram, points Q_4, Q_5 and Q_6 can be ignored.

Following characteristics should also be noted with respect to a plot between $\ddot{s}(t)$ vs. $s(t)$,

(i.) Corresponding values of s-axis of the graph cannot be extended or retracted as whole, since the initial and final points are fixed at s = 0 and s = 1 respectively. However, by means of adjusting p and T, s-axis values can be moved within the range of 0 and 1.

(ii.) Area covered by the top part of a $\ddot{s}(t)$ vs. $s(t)$ graph is equal to :

$$\int_0^{(p/T)} \ddot{s}ds = \int_0^{(2/T)} \frac{dv}{dt}(v.dt) = \int_0^{(2/T)} vdv = 2/T^2 \qquad (10)$$

Where $v = \frac{ds}{dt}$.

Value found in (10) is equal to half of the square of velocity gained during acceleration. Note that since velocity gained during acceleration is exactly equal to velocity seized during deceleration, area covered by the bottom part of the graph is equal to the negative value of the area covered by the top part of the graph. In figure 3.4, area of the polygon $Q_1Q_2Q_3Q_5$ is equal to $\frac{40}{18T^2}$; which is an approximation of actual value $\frac{2}{T^2}$. Area of polygon $Q_5Q_7Q_8Q_9$ is also equal to $\frac{40}{18T^2}$ with a negative sign. Note that, the value $\frac{40}{18T^2}$ is a variable in T (and T only) regardless of any other characteristic of the graph. Higher this value, lesser the value of T, which is the total duration. Therefore, optimizing (minimizing) the total duration will require maximizing the area $Q_1Q_2Q_3Q_5$. Any constraint imposed on increasing this area should be considered during this maximization. Since area $Q_5Q_7Q_8Q_9$ is also increasing during such a maximization any constraint(s) imposed on maximizing area

$Q_5Q_7Q_8Q_9$ should also be considered simultaneously during such a maximization.

3.4 Application of S-Model in FAD and obtaining results

It was emphasized in chapter 2, that the kinematics of EE $\{\ddot{X}(t)$ vs. $X(t)\}$ shall be limited by all the lower bounds of FAD in order to maintain positive tension in cables at all times. To find these limitations with respect to the behavior of EE developed S-Model will now be applied in Equations of lower bounds of respective FADs for 2-DOF (Planar), 3-Cable and 3-DOF (Planar), 4-Cable configurations.

3.4.1 Application of S-Model in 3-DOF (spatial), 4-Cable configuration

First, the model will be applied on spatial – 4 cable case.

Substituting (7) and (9) in (3) to (6), following equations can be obtained:

$$(z_1 - z_0)\ddot{s} \geq \frac{z_{max} - \{z_0 + (z_1 - z_0)s\}}{-\{y_0 + (y_1 - y_0)s\}}(y_1 - y_0)\ddot{s} - g \quad (11)$$

$$(z_1 - z_0)\ddot{s} \geq \frac{z_{max} - \{z_0 + (z_1 - z_0)s\}}{x_{max} - \{x_0 + (x_1 - x_0)s\}}(x_1 - x_0)\ddot{s} - g \quad (12)$$

$$(z_1 - z_0)\ddot{s} \geq \frac{z_{max} - \{z_0 + (z_1 - z_0)s\}}{y_{max} - \{y_0 + (y_1 - y_0)s\}}(y_1 - y_0)\ddot{s} - g \quad (13)$$

$$(z_1 - z_0)\ddot{s} \geq \frac{z_{max} - \{z_0 + (z_1 - z_0)s\}}{-\{x_0 + (x_1 - y_0)s\}}(x_1 - x_0)\ddot{s} - g \quad (14)$$

Note that, values $-\{y_0 + (y_1 - y_0)s\}$and $-\{x_0 + (x_1 - x_0)s\}$are always negative, whereas values $x_{max} - \{x_0 + (x_1 - x_0)s\}$and $y_{max} - \{y_0 + (y_1 - y_0)s\}$are always positive since the EE is inside the footprint of robot. Considering this, following inequalities can be obtained.

$\ddot{s}(t) \leq g\frac{(y_1 - y_0)}{K_1}s(t) + g\frac{y_0}{K_1}$for $K_1 > 0$, and (15)

$\ddot{s}(t) \geq g\frac{(y_1 - y_0)}{K_1}s(t) + g\frac{y_0}{K_1}$for $K_1 < 0$

where $K_1 = [(z_1 - z_0)(-y_0) - (z_{max} - z_0)(y_1 - y_0)]$

$\ddot{s}(t) \geq g\frac{(x_1 - x_0)}{K_2}s(t) - g\frac{(x_{max} - x_0)}{K_2}$for $K_2 > 0$, and (16)

$\ddot{s}(t) \leq g\frac{(x_1-x_0)}{K_2}s(t) - g\frac{(x_{max}-x_0)}{K_2}$ for K_2 <0

where$K_2 = [(z_1 - z_0)(x_{max} - x_0) - (z_{max} - z_0)(x_1 - x_0)]$

$\ddot{s}(t) \geq g\frac{(y_1-y_0)}{K_3}s(t) - g\frac{(y_{max}-y_0)}{K_3}$ for K_3 >0, and (17)

$\ddot{s}(t) \leq g\frac{(y_1-y_0)}{K_3}s(t) - g\frac{(y_{max}-y_0)}{K_3}$ for K_3 <0

where$K_3 = [(z_1 - z_0)(y_{max} - y_0) - (z_{max} - z_0)(y_1 - y_0)]$

$\ddot{s}(t) \leq g\frac{(x_1-x_0)}{K_4}s(t) + g\frac{x_0}{K_4}$ for K_4 >0, and (18)

$\ddot{s}(t) \geq g\frac{(x_1-x_0)}{K_4}s(t) + g\frac{x_0}{K_4}$ for K_4 <0

where$K_4 = [(z_1 - z_0)(-x_0) - (z_{max} - z_0)(x_1 - x_0)]$

3.4.2 Application of S-Model in 2-DOF (Planar), 3-Cable configuration

Substituting (7) and (9) in (2) following equation could be obtained.

$(z_1 - z_0)\ddot{s} \geq \frac{w-\{z_0-(z_1-z_0)s\}}{p_i-\{x_0-(x_1-x_0)s\}}(x_1 - x_0)\ddot{s} - g$ (19)

where *i* refers to the cables' directions and $p_1 = 0$, $p_2 = u_1$, $p_3 = u_2$. Note that, the value of $p_i - \{x_0 - (x_1 - x_0)s\}$ is always negative for $p_1 = 0$; whereas, the value of it is always positive for $p_2 = u_1$, $p_3 = u_2$. Further, according to the configuration (figure 2.5), and corresponding FAD (figure 2.6), it is sufficient to satisfy only the inequalities for *i = 1* and *i = 3*.

This yields to development of two inequalities:-

$\ddot{s}(t) \leq g\frac{(x_1-x_0)}{K_1}s(t) + g\frac{x_0}{K_1}$ for K_1>0, and (20)

$\ddot{s}(t) \geq g\frac{(x_1-x_0)}{K_1}s(t) + g\frac{x_0}{K_1}$ for K_1<0

where, $K_i = [(z_1 - z_0)(-x_0) - (z_{max} - z_0)(x_1 - x_0)]$

and

$\ddot{s}(t) \geq g\frac{(x_1-x_0)}{K_3}s(t) - g\frac{(x_{max}-x_0)}{K_3}$ for K_1>0, and (21)

$\ddot{s}(t) \leq g\frac{(x_1-x_0)}{K_3}s(t) - g\frac{(x_{max}-x_0)}{K_3}$ for $K_3<0$

where, $K_3 = [(z_1 - z_0)(x_{max} - x_0) - (w - z_0)(x_1 - x_0)]$

This shows that several inequalities can be developed for any given 2DOF 3-cable or 3DOF 4-cable system. When these inequalities are plotted as $\ddot{s}(t)$ vs. $s(t)$, they will represent straight-line boundaries. Further to these boundaries, additional boundaries can be introduced by considering safe acceleration and deceleration values for entire trajectory. All these boundaries shall be considered during maximization of area $Q_1Q_2Q_3Q_5$ discussed in section 3.4.1. This procedure will be discussed in detail during the experiment in Section-4.

4. EXPERIMENTAL SETUP

This section illustrates the experiment carried out for 3DOF scenario by applying the theory developed in chapter 3. Results will be verified by simulations.

Test Case: Generation of Time optimized smooth trajectory for EE from point B_0 to point B_1 in following 3DOF case.

With reference to figure 1.2 and section 3.2, Coordinates of the four corners of the top base of the robot are:

$A_1 \equiv (0, 0, z_{max}) \equiv (0,0,30)$,

$A_2 \equiv (x_{max}, 0, z_{max}) \equiv (45,0,30)$,

$A_3 \equiv (x_{max}, y_{max}, z_{max}) \equiv (45,30,30)$,

$A_3 \equiv (0, y_{max}, z_{max}) \equiv (0,30,30)$,

Initial position of EE: $B_0 \equiv (x_0, y_0, z_0) \equiv (1,20,7)$

Final position of EE: $B_1 \equiv (x_1, y_1, z_1) \equiv (15,28,3)$,

Maximum acceleration/deceleration (along the straight-line trajectory) allowed to avoid unsafe operations: 10 ms^{-2}

All dimensions are in standard SI units. Gravitational acceleration is 9.81 ms^{-2}.

4.1. Application of the theory developed and obtaining the parameters of the trajectory

Four inequalities calculated by substituting values of test case-1 in inequalities (15) to (18) are given below:

$$\ddot{s} \geq -0.755s - 1.887 \quad (22)$$

$$\ddot{s} \leq -0.276s + 0.867 \quad (23)$$

$$\ddot{s} \leq -0.350s + 0.438 \quad (24)$$

$$\ddot{s} \geq -0.432s - 0.031 \quad (25)$$

Total distance (d) of the trajectory calculated using coordinates of B_0 and B_1 = 16.613

By equation (9), magnitude of acceleration can be calculated as below:

$$|\ddot{X}(t)| = |(X_1 - X_0)\ddot{s}(t)| \leq 10$$

$$\sqrt{\{(x_1 - x_0)\ddot{s}(t)\}^2 + \{(y_1 - y_0)\ddot{s}(t)\}^2 + \{(z_1 - z_0)\ddot{s}(t)\}^2} \leq 10$$

By substituting coordinate values;

$$\ddot{s}(t) \leq 0.602 \quad (26)$$

$$\ddot{s}(t) \geq -0.602 \quad (27)$$

Figure 4.1 shows the plot of inequalities (22) to (27) in $\ddot{s}(t)$ vs. $s(t)$.

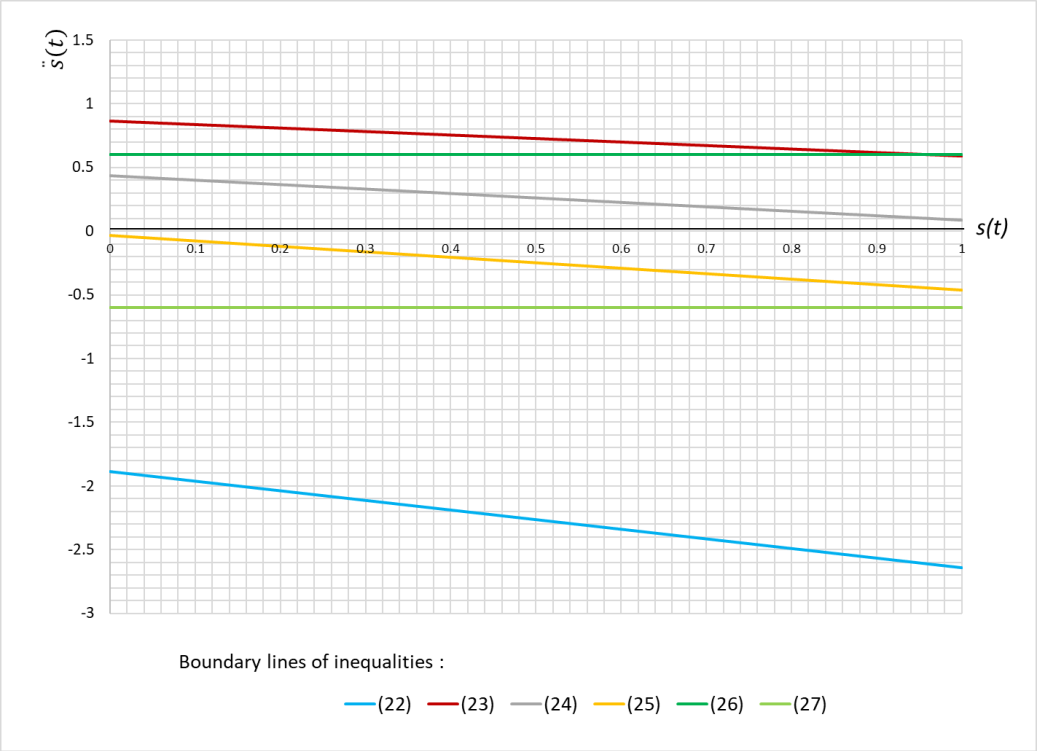

Figure 4.1: plot of inequalities (22) to (27) in $\ddot{s}(t)$ vs. $s(t)$

Area within boundaries of (24) and (25) satisfy all inequalities. Recalling the Q-points discussed in section-3. As mentioned in sections 3.41 and 3.4.2, in order to optimize T, area of polygon $Q_1Q_2Q_3Q_5$ (see figure 3.4) shall be maximized. Since boundary of (24) is limiting this maximization it shall be considered as the constraint on increasing the area $Q_1Q_2Q_3Q_5$. While doing this, $Q_5Q_7Q_8Q_9$ will also increase. Therefore, the boundary of (25) shall be considered parallelly as the constraint on increasing the area $Q_5Q_7Q_8Q_9$. T shall be noted that area $Q_1Q_2Q_3Q_5$ can be enlarged in both positive direction of *s* as well as $\ddot{s}$. Consider increasing the area in positive direction of $\ddot{s}$. Since the gradient of boundary of (24) is negative, the only Q-point, which can 'touch' the boundary of (24) is $Q_3 = (\frac{p}{6T}, \frac{4}{Tp})$. Substituting these variables in the boundary of (24):

Therefore, $\frac{4}{Tp} = -\frac{0.350(p)}{(6T)} + 0.438$ (28)

Consider increasing the area $Q_1Q_2Q_3Q_5$ in the positive direction of *s*. In case the gradient of boundary of (24) was positive, moving point Q_3 along this limit towards the positive direction of *s* will increase the area $Q_1Q_2Q_3Q_5$ indefinitely until any constraint imposed on bottom part of the graph limits the area $Q_5Q_7Q_8Q_9$. Boundary of (25) limits the area $Q_5Q_7Q_8Q_9$. Since the gradient of (25) is negative the only Q point that can 'touch' the boundary of (25) is $Q_7 = (\frac{p}{6T} + \frac{5}{6}, -\frac{4}{T(T-p)})$. Substituting these variables in the boundary of (25):

$$-\frac{4}{T(T-p)} = -0.432(\frac{p}{6T} + \frac{5}{6}) - 0.031 \quad (29)$$

Thus, when both: point Q_3 lies on the boundary of (24) and Q_7 lies on the boundary of (25) simultaneously both areas $Q_1Q_2Q_3Q_5$ and $Q_5Q_7Q_8Q_9$ reaches their maximum values. Thus, T is optimal. T and p values can be found by solving equations (28) and (29). Say the *s* value of Q_3 calculated by substituting the T and p found is s_{top_opt1}. In the test case a secondary issue has to be considered since the gradient of boundary (24) is negative. Due to this, area $Q_1Q_2Q_3Q_5$ may not increase indefinitely until Q_7 touches (25) while moving Q_3 along the positive direction of *s*. Since the gradient of boundary of (24) is negative, there is a possibility that the maximum of $Q_1Q_2Q_3Q_5$ be reached before Q_7 touches the boundary of (25). i.e. a different *s* value prior to reaching s_{top_opt1}. Say the *s* value of Q_3 at this point is s_{top_opt2}. To find the correct optimal T, first both s_{top_opt1} and s_{top_opt2} shall be calculated. Then T value corresponding to lesser *s* (out of s_{top_opt1} *and* s_{top_opt}) should be considered as the correct optimal T. Therefore, for the test case the values of p and T corresponding to point s_{top_opt1} will be found first. These values will be labelled as p_1 and T_1. Table 4.1 shows the values were obtained for p_1 and T_1 by solving (28) and (29) simultaneously.

Table 4.1: P_1 and T_1 values of case-1

	T_1	**P_1**
Solution 1	-0.138i	-7.774i
Solution 2	+0.138i	+7.774i
Solution 3	- 4.377	-2.240
Solution 4	+4.377	+2.240

The valid solution is p_1 = +2.240, and T_1 = +4.377.

Calculated s_{top_opt1} = 0.085

Now, p and T values corresponding to s_{top_opt2} will be found. These are labelled as p_2 and T_2.

From (28),

$$(\frac{1}{{T_2}^2}) = -0.01458(\frac{p_2}{T_2})^2 + 0.1095(\frac{p_2}{T_2}) \quad (30)$$

This is a $y = -ax^2 + bx$ type of an expression with maximum value of y ($= \frac{1}{{T_2}^2}$) is reached at $x = \frac{b}{2a}$. Substituting this in (24), the value obtained for $(\frac{p_2}{T_2})$ = 3.755.

Calculated s_{top_opt2} = 0.626.

Since $s_{top\_opt1} < s_{top\_opt2}$ T = 4.377 (s) and p = 2.24 (s) corresponds to an optimum time duration.

Behavior of $\ddot{s}(t)$ calculated using table 3.2 are given in table 4.2.

Table 4.2: Behavior of $\ddot{s}(t)$ in test case

t (seconds)	$\ddot{s}(t)$
$0 \leq t < 1.120$	0.364*t*
$1.120 \leq t < 2.240$	0.816 – 0.364*t*
$2.240 \leq t < 3.308$	0.896 – 0.400*t*
$3.308 \leq t \leq 4.377$	0.400*t* – 1.752

4.2 Simulation of results

Trajectory has been simulated for $0 \leq t \leq T$ based on parameters obtained for test case in section 4.1 to obtain following profiles:

1. Displacement vs. Time in directions parallel to three axis and overall displacement for
2. Acceleration vs. Time in directions parallel to three axis and Resultant acceleration
3. Verification of inequalities (3) to (6)
4. Magnitude of tension couples

Then a numerical method has been used to verify if the duration, T found is in fact the optimal duration.

4.2.1 Displacement vs. Time

Behavior functions of $s(t)$ can be found by substituting the optimal T and p values found in section 4.1 in table 3.2. Displacement in each direction X, Y and Z can be found by substituting these functions in equation (7). Profile of displacement of EE in directions X, Y and Z from their respective initial values and along the straight line it traversed are plotted in figure 4.2. The total distance traversed is 16.61 m. Average velocity during the traverse is 3.79 ms^{-1}.

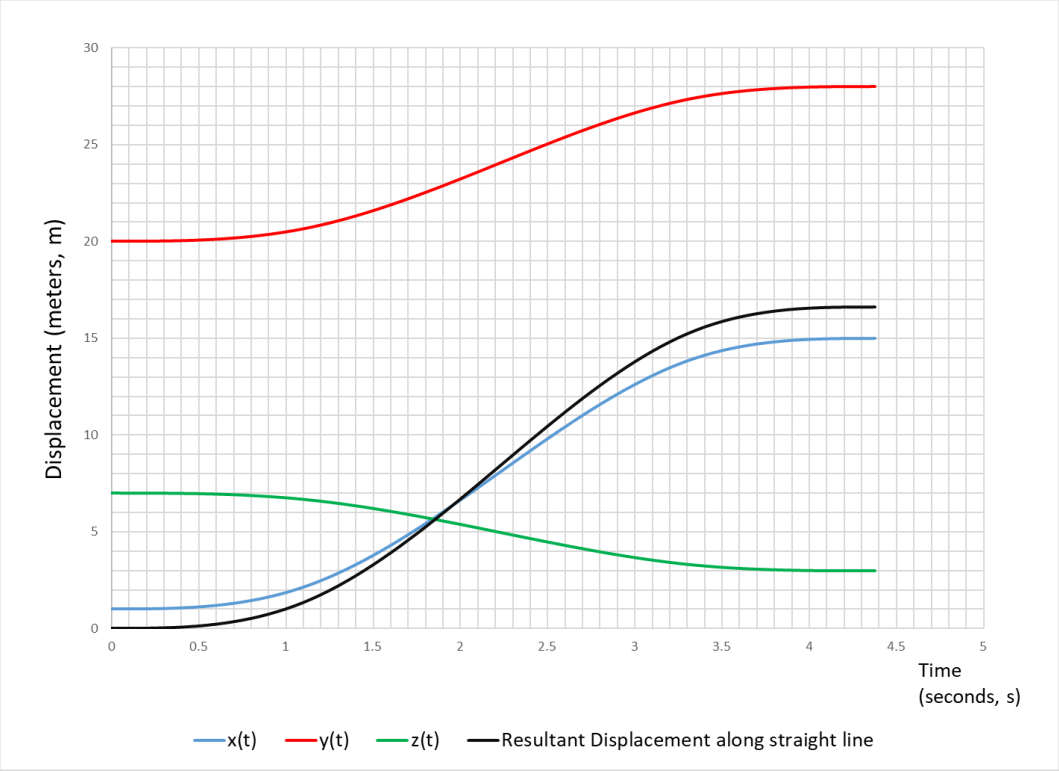

Figure 4.2: Profile of the displacement of EE

4.2.2 Acceleration vs. Time

Behavior of acceleration of EE in directions X, Y and Z can be found by substituting functions found in table 4.2 in equation (9). Profile of acceleration of EE in directions X, Y and Z and along the straight line it traversed are plotted in figure 4.3. This plot shows that first, the resultant acceleration increases from zero to its maximum value 6.78 ms^{-2}, and then decreases back to zero. From there the deceleration increases up to 7.10 ms^{-2} and reduces back to zero.

4.2.3 Verification of feasibility of acceleration

As mentioned in section 2.4, if the acceleration vector lies inside the inverted pyramid shape developed in FAD there exists a combination of non-negative cable tensions that can provide that acceleration. Conversely, if the acceleration vector breaches these boundary limits at least one tension shall be negative in order to provide that acceleration. Therefore, $(\ddot{x}, \ddot{y}, \ddot{z})$ being inside the edges of the said inverted pyramid at all times during the trajectory is the necessary and sufficient condition for feasible accelerations. In order to verify if this condition is satisfied or not inequalities (3) to (6) were deducted. For feasible trajectories, Left hand side (LHS) value in each inequality shall be larger or equal to the right hand side (RHS) value. These conditions are verified in figures 4.4 (a), 4.4 (b), 4.4 (c) and 4.4 (d).

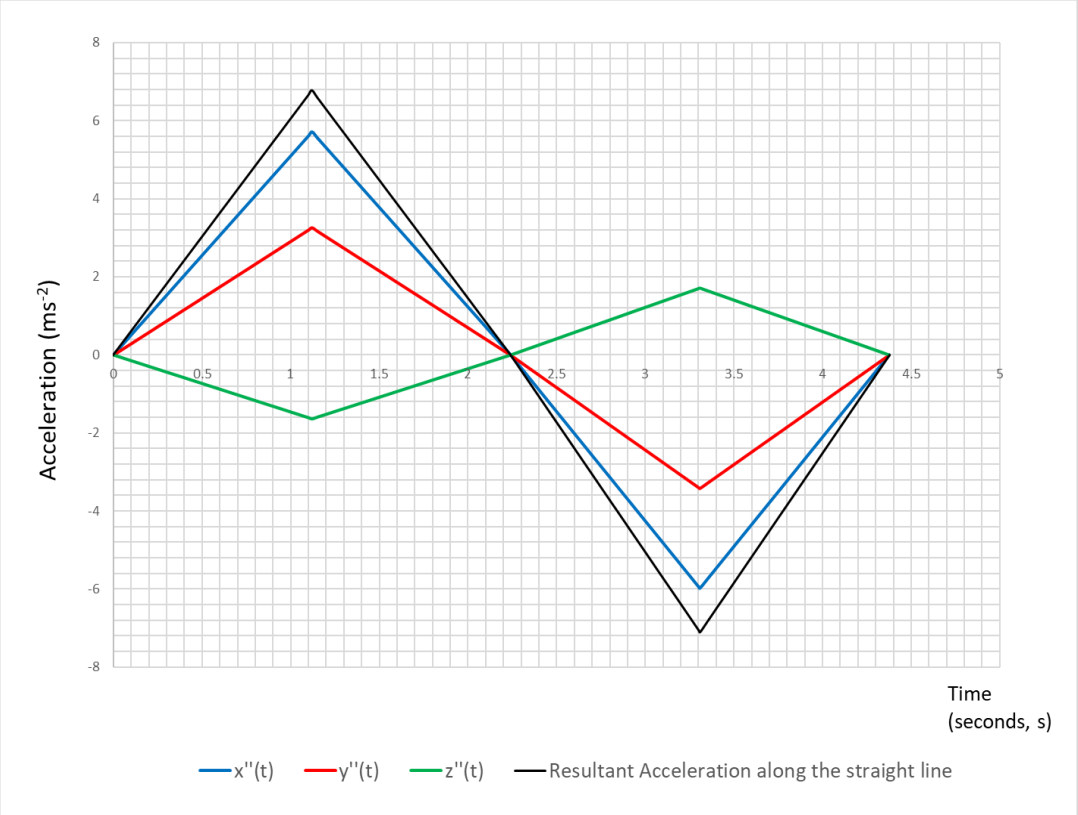

Figure 4.3: Profile of the acceleration of EE

Figure 4.4 (a): Verification of Inequality (3)

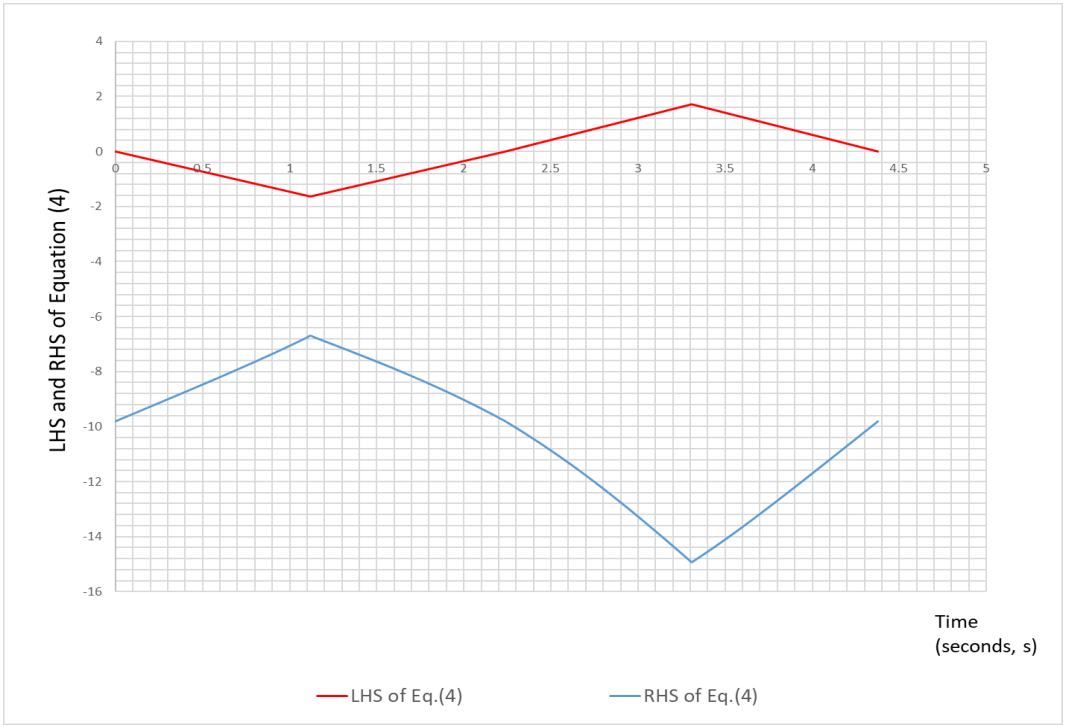

Figure 4.4 (b): Verification of Inequality (4)

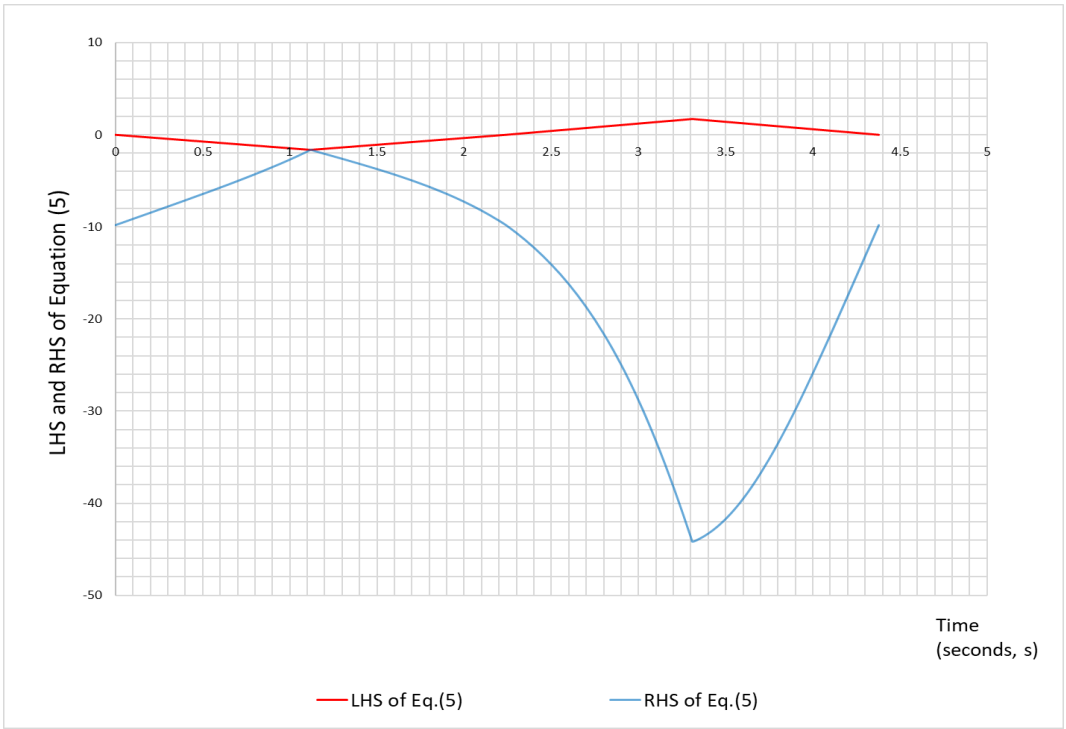

Figure 4.4 (c): Verification of Inequality (5)

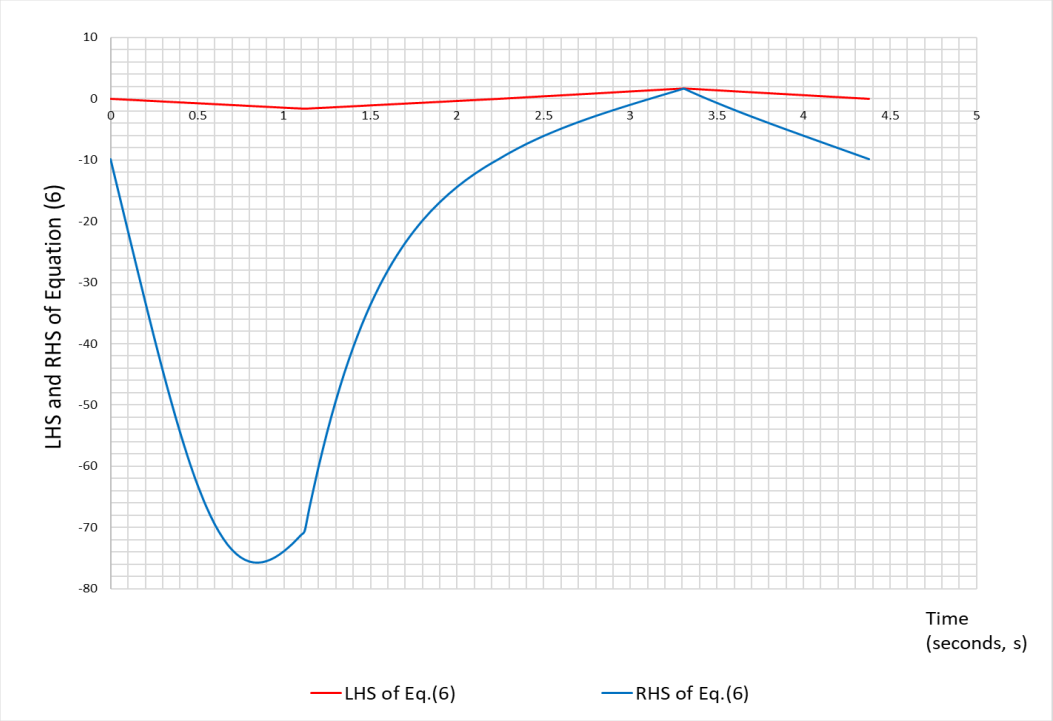

Figure 4.4 (d): Verification of Inequality (6)

figures 18(a) to 18(d) show that all inequalities are satisfied. Further, recall from section 4.1, the two inequalities applicable to restrain the motion were (24) and (25) deducted from (5) and (6) respectively. Therefore, as it should be the case, it can be clearly seen that LHS and RHS values of graphs in figures 4.4 (c) and 4.4 (d) corresponding to (5) and (6) close at two different point of time, at 1.120 s and at 3.308 s respectively.

4.2.4 Magnitudes of tension couples

As mentioned in section 1.2, the tensions of the cables in 3DoF (spatial) – 4 cable case are indeterministic. However, the summation of tension components of each sequential couple of cables (Eg:- summation of tension components of cables 1 and 2 in in X-Z plane) can be found by applying motion equations. These values, which will hereafter be termed as 'tension couples' are given in equations (30) to (33). The deduction of these equations are given in Appendix C.

Tension couple 1 : $T_{1,2} = m\frac{(\ddot{z}+g)(y_{max}-y)-\ddot{y}(z_{max}-z)}{y_{max}(z_{max}-z)}\sqrt{y^2+(z_{max}-z)^2}$ (30)

Tension couple 2 : $T_{2,3} = m\frac{(\ddot{z}+g)x+\ddot{x}(z_{max}-z)}{y_{max}(z_{max}-z)}\sqrt{(x_{max}-x)^2+(z_{max}-z)^2}$ (31)

Tension couple 3 : $T_{3,4} = m\frac{(\ddot{z}+g)y+\ddot{y}(z_{max}-z)}{y_{max}(z_{max}-z)}\sqrt{(y_{max}-y)^2+(z_{max}-z)^2}$ (32)

Tension couple 4 : $T_{4,1} = m\frac{(\ddot{z}+g)(x_{max}-x)-\ddot{x}(z_{max}-z)}{x_{max}(z_{max}-z)}\sqrt{x^2+(z_{max}-z)^2}$ (33)

Values of these tension couples for case-1 were calculated and plotted for a mass of EE = 10 kg, and the same are given in figures 4.5 (a) to 4.5 (d). The forces are in Newtons and the time is in seconds.

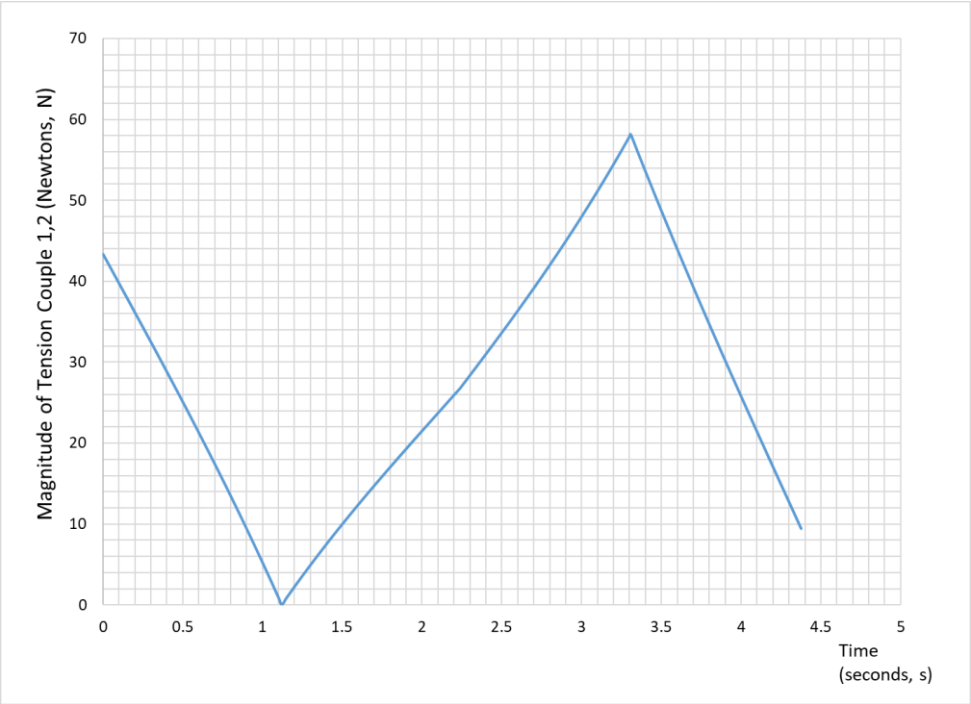

Figure 4.5 (a): Magnitude of Tension Couple 1,2

Graphs plotted shown in figures 4.5 (a) to 4.5 (d) illustrate that in each case, tension couples are non-negative. All the tensions lie within zero and 130 N.

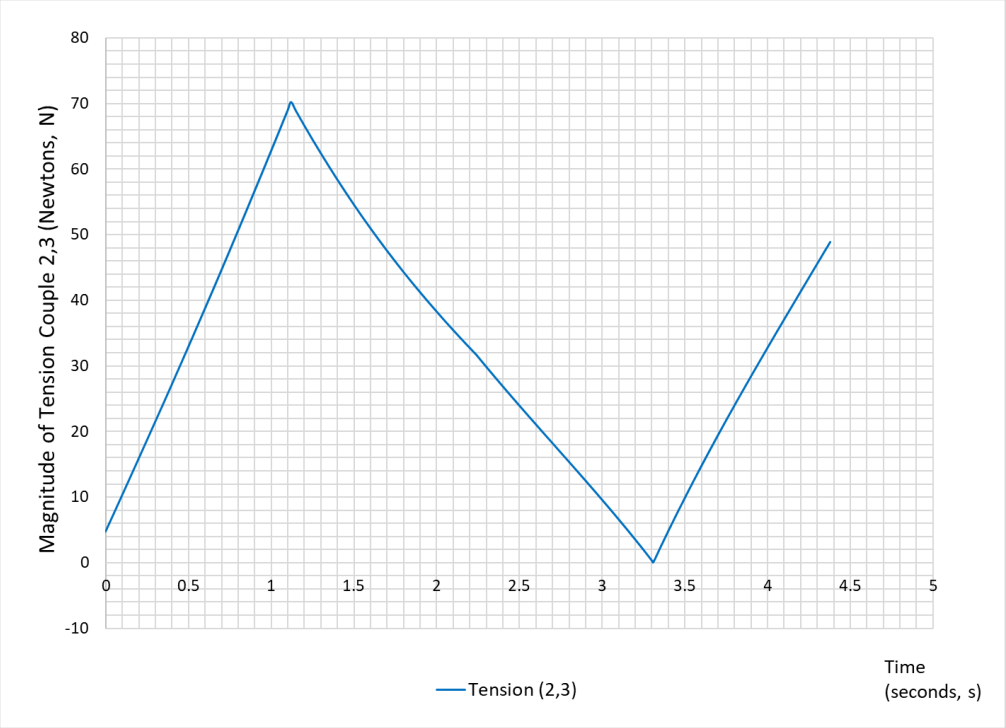

Figure 4.5 (b): Magnitude of Tension Couple 2,3

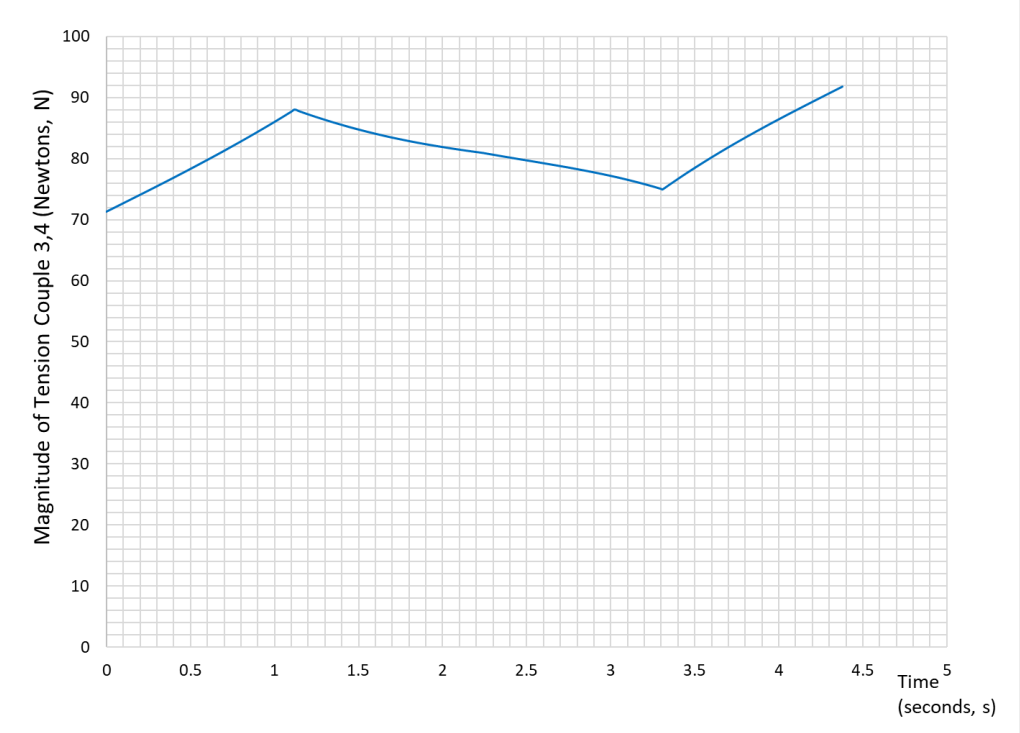

Figure 4.5 (c): Magnitude of Tension Couple 3,4

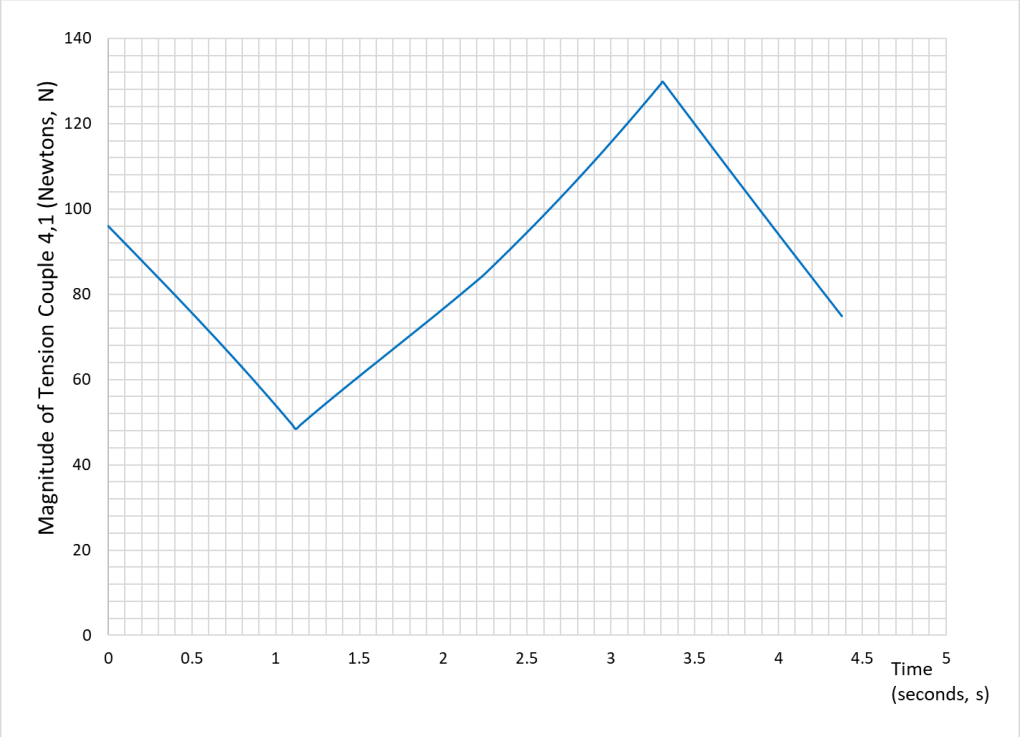

Figure 4.5 (d): Magnitude of Tension Couple 4,1

4.2.5 Verification of optimum duration

In order to verify if the duration found in test case is the optimum, following procedure is used.

For the test case following values were calculated in the increments of 0.05 (s) for p and T.

(a.) Max_a : Maximum of $\{f_{traj}(s) - f_+(s)\}$ for each p and T

where 0 < T < (Optimum found in section-4) and 0 < p < T.

(b.) Max_b : Maximum of $\{f_-(s) - f_{traj}(s)\}$ for each p and T

where 0 < T < (Optimum found in secion-4) and 0 < p < T. where, $f_{traj}(s)$ is the value obtained for $\ddot{s}$ from s-model for a particular set of T, p and s. Upper limit of T for which the values are calculated in this exercise is the optimum T value found for each case in section-4, since the purpose is to check if there is a lesser T value.

$f_+(s)$ is the value obtained for $\ddot{s}$from acceleration side bound for each s, and $f_-(s)$ is the value obtained for $\ddot{s}$from deceleration side bound for each s. It shall be noted that,

feasible dynamics exist for any set of T and p values for which both Max_a and max_b are negative. The objective is to find the minimum T value and corresponding p value which satisfies this condition.

Numerical results for case-1 yielded a minimum T value and a corresponding p value at T= 4.35 and p = 2.25 whereas, the solution found in section-3 is T = 4.377, p = 2.24.

Table 4.3 (a) and Table 4.3 (b) show the variation of Max_a and Max_b at the close vicinity of the values found in test case ($2.90 < T < 4.40$ and $1.80 < p < 2.75$). In each table, negative values are highlighted and trend of negative values can be seen. From these tables, minimum T value and corresponding p value for which both Max_a and Max_b values are negative, can be easily selected.

		p value(s)																		
		1.8	1.85	1.9	1.95	2	2.05	2.1	2.15	2.2	2.25	2.3	2.35	2.4	2.45	2.5	2.55	2.6	2.65	2.7	2.75
T value (s)	2.9	0.3646	0.3449	0.3263	0.3087	0.2920	0.2762	0.2611	0.2469	0.2333	0.2204	0.2081	0.1963	0.1851	0.1744	0.1641	0.1543	0.1449	0.1359	0.1273	0.1190
	2.95	0.3510	0.3316	0.3133	0.2960	0.2796	0.2641	0.2493	0.2353	0.2219	0.2092	0.1971	0.1856	0.1745	0.1640	0.1539	0.1443	0.1350	0.1262	0.1177	0.1096
	3	0.3378	0.3188	0.3008	0.2838	0.2676	0.2524	0.2378	0.2241	0.2109	0.1984	0.1865	0.1752	0.1643	0.1540	0.1440	0.1346	0.1255	0.1168	0.1084	0.1004
	3.05	0.3251	0.3064	0.2887	0.2719	0.2561	0.2410	0.2268	0.2132	0.2003	0.1880	0.1763	0.1651	0.1544	0.1443	0.1345	0.1252	0.1162	0.1077	0.0995	0.0916
	3.1	0.3128	0.2944	0.2770	0.2605	0.2449	0.2301	0.2160	0.2027	0.1900	0.1779	0.1664	0.1554	0.1449	0.1349	0.1253	0.1161	0.1073	0.0989	0.0908	0.0831
	3.15	0.3009	0.2827	0.2656	0.2494	0.2340	0.2195	0.2057	0.1925	0.1800	0.1681	0.1568	0.1460	0.1356	0.1258	0.1163	0.1073	0.0986	0.0904	0.0824	0.0748
	3.2	0.2893	0.2715	0.2546	0.2387	0.2235	0.2092	0.1956	0.1827	0.1704	0.1587	0.1475	0.1368	0.1267	0.1170	0.1077	0.0988	0.0903	0.0821	0.0743	0.0668
	3.25	0.2782	0.2606	0.2440	0.2282	0.2134	0.1993	0.1859	0.1731	0.1610	0.1495	0.1385	0.1280	0.1180	0.1084	0.0993	0.0905	0.0821	0.0741	0.0664	0.0590
	3.3	0.2673	0.2500	0.2336	0.2182	0.2035	0.1896	0.1764	0.1639	0.1519	0.1406	0.1298	0.1194	0.1096	0.1001	0.0911	0.0825	0.0743	0.0663	0.0588	0.0515
	3.35	0.2568	0.2397	0.2236	0.2084	0.1939	0.1802	0.1672	0.1549	0.1431	0.1319	0.1213	0.1111	0.1014	0.0921	0.0832	0.0747	0.0666	0.0588	0.0513	0.0442
	3.4	0.2466	0.2298	0.2139	0.1989	0.1846	0.1711	0.1583	0.1462	0.1346	0.1236	0.1131	0.1030	0.0935	0.0843	0.0756	0.0672	0.0592	0.0515	0.0442	0.0371
	3.45	0.2366	0.2201	0.2044	0.1896	0.1756	0.1623	0.1497	0.1377	0.1263	0.1154	0.1051	0.0952	0.0858	0.0768	0.0681	0.0599	0.0520	0.0444	0.0372	0.0302
	3.5	0.2270	0.2107	0.1953	0.1807	0.1668	0.1537	0.1413	0.1295	0.1182	0.1075	0.0973	0.0876	0.0783	0.0694	0.0609	0.0528	0.0450	0.0375	0.0304	0.0235
	3.55	0.2176	0.2015	0.1863	0.1720	0.1583	0.1454	0.1331	0.1215	0.1104	0.0998	0.0898	0.0802	0.0710	0.0623	0.0539	0.0459	0.0382	0.0308	0.0238	0.0170
	3.6	0.2085	0.1927	0.1777	0.1635	0.1500	0.1373	0.1252	0.1137	0.1028	0.0924	0.0824	0.0730	0.0639	0.0553	0.0470	0.0391	0.0316	0.0243	0.0174	0.0107
	3.65	0.1997	0.1840	0.1692	0.1552	0.1420	0.1294	0.1175	0.1062	0.0954	0.0851	0.0753	0.0660	0.0571	0.0485	0.0404	0.0326	0.0251	0.0180	0.0111	0.0046
	3.7	0.1911	0.1756	0.1610	0.1472	0.1342	0.1218	0.1100	0.0988	0.0882	0.0780	0.0684	0.0592	0.0504	0.0420	0.0339	0.0262	0.0189	0.0118	0.0051	-0.0014
	3.75	0.1827	0.1674	0.1530	0.1394	0.1265	0.1143	0.1027	0.0917	0.0812	0.0712	0.0616	0.0525	0.0439	0.0356	0.0276	0.0201	0.0128	0.0058	-0.0008	-0.0072
	3.8	0.1745	0.1595	0.1453	0.1318	0.1191	0.1070	0.0956	0.0847	0.0743	0.0645	0.0551	0.0461	0.0375	0.0293	0.0215	0.0140	0.0069	0.0000	-0.0066	-0.0129
	3.85	0.1666	0.1517	0.1377	0.1244	0.1119	0.1000	0.0886	0.0779	0.0677	0.0579	0.0487	0.0398	0.0314	0.0233	0.0156	0.0082	0.0011	-0.0057	-0.0122	-0.0184
	3.9	0.1588	0.1441	0.1303	0.1172	0.1048	0.0931	0.0819	0.0713	0.0612	0.0516	0.0424	0.0337	0.0253	0.0174	0.0097	0.0024	-0.0045	-0.0112	-0.0177	-0.0238
	3.95	0.1512	0.1368	0.1231	0.1102	0.0979	0.0863	0.0753	0.0648	0.0549	0.0454	0.0363	0.0277	0.0195	0.0116	0.0041	-0.0031	-0.0100	-0.0166	-0.0230	-0.0291
	4	0.1439	0.1296	0.1161	0.1033	0.0912	0.0798	0.0689	0.0586	0.0487	0.0393	0.0304	0.0219	0.0138	0.0060	-0.0015	-0.0086	-0.0154	-0.0219	-0.0282	-0.0342
	4.05	0.1367	0.1226	0.1093	0.0967	0.0847	0.0734	0.0626	0.0524	0.0427	0.0334	0.0246	0.0162	0.0082	0.0005	-0.0068	-0.0139	-0.0206	-0.0270	-0.0332	-0.0392
	4.1	0.1297	0.1158	0.1026	0.0901	0.0783	0.0672	0.0565	0.0464	0.0368	0.0277	0.0190	0.0107	0.0027	-0.0048	-0.0121	-0.0190	-0.0257	-0.0321	-0.0382	-0.0440
	4.15	0.1229	0.1091	0.0961	0.0838	0.0721	0.0611	0.0506	0.0406	0.0311	0.0221	0.0135	0.0053	-0.0026	-0.0101	-0.0172	-0.0241	-0.0307	-0.0369	-0.0430	-0.0488
	4.2	0.1162	0.1026	0.0897	0.0776	0.0660	0.0551	0.0448	0.0349	0.0255	0.0166	0.0081	0.0000	-0.0078	-0.0152	-0.0222	-0.0290	-0.0355	-0.0417	-0.0477	-0.0534
	4.25	0.1097	0.0962	0.0835	0.0715	0.0601	0.0493	0.0391	0.0293	0.0201	0.0113	0.0029	-0.0052	-0.0128	-0.0201	-0.0271	-0.0338	-0.0402	-0.0464	-0.0523	-0.0579
	4.3	0.1033	0.0900	0.0774	0.0656	0.0543	0.0437	0.0335	0.0239	0.0148	0.0060	-0.0023	-0.0102	-0.0178	-0.0250	-0.0319	-0.0385	-0.0449	-0.0509	-0.0568	-0.0623
	4.35	0.0971	0.0839	0.0715	0.0598	0.0487	0.0381	0.0281	0.0186	0.0096	0.0009	-0.0073	-0.0151	-0.0226	-0.0297	-0.0366	-0.0431	-0.0494	-0.0554	-0.0611	-0.0667
	4.4	0.0910	0.0780	0.0657	0.0541	0.0431	0.0327	0.0228	0.0134	0.0045	-0.0040	-0.0122	-0.0199	-0.0273	-0.0344	-0.0411	-0.0476	-0.0538	-0.0597	-0.0654	-0.0709

Table 4.3 (a) : Test Case Numerical results of Max_a
for $2.90 < T < 4.40$ and $1.80 < p < 2.75$

		p value(s)																			
		1.8	1.85	1.9	1.95	2	2.05	2.1	2.15	2.2	2.25	2.3	2.35	2.4	2.45	2.5	2.55	2.6	2.65	2.7	2.75
T value (s)	2.9	0.81848	0.87695	0.94139	1.01275	1.09217	1.18108	1.28125	1.39496	1.52508	1.67541	1.851	2.05875	2.30829	2.61356	2.99546	3.48683	4.14241	5.06071	6.43878	8.73639
	2.95	0.74439	0.79677	0.85424	0.91759	0.98774	1.06581	1.15321	1.2517	1.36347	1.49139	1.63917	1.81179	2.01601	2.26132	2.56142	2.93685	3.41989	4.06435	4.96709	6.3218
	3	0.67716	0.72427	0.77577	0.83229	0.89459	0.96356	1.04034	1.12628	1.22312	1.33303	1.45882	1.60414	1.77388	1.9747	2.21592	2.51102	2.88019	3.35518	3.9889	4.87659
	3.05	0.61594	0.65848	0.70481	0.75547	0.81106	0.87234	0.94018	1.0157	1.10023	1.19548	1.30359	1.42732	1.57025	1.73721	1.93474	2.17201	2.46227	2.82539	3.29259	3.91592
	3.1	0.56	0.59854	0.64039	0.68598	0.73582	0.79052	0.8508	0.91755	0.99185	1.07502	1.16874	1.27511	1.39683	1.53746	1.70173	1.89607	2.12952	2.41509	2.77235	3.23202
	3.15	0.50873	0.54377	0.5817	0.62288	0.66775	0.7168	0.77063	0.82995	0.89564	0.96876	1.05061	1.14284	1.24752	1.36731	1.50572	1.66737	1.85863	2.08837	2.36941	2.721
	3.2	0.46161	0.49355	0.52804	0.56538	0.60592	0.65008	0.69837	0.75136	0.80975	0.87442	0.94639	1.02697	1.11776	1.2208	1.33872	1.47496	1.63409	1.82236	2.04851	2.32516
	3.25	0.41818	0.44739	0.47884	0.5128	0.54956	0.58948	0.63296	0.6805	0.73268	0.79018	0.85385	0.92471	1.00405	1.09344	1.1949	1.31101	1.44515	1.60183	1.7872	2.00987
	3.3	0.37806	0.40483	0.4336	0.46457	0.49802	0.53422	0.57354	0.61636	0.66318	0.71456	0.77119	0.8339	0.90369	0.98183	1.06986	1.16978	1.28413	1.41624	1.57055	1.75311
	3.35	0.34091	0.36551	0.39189	0.42022	0.45073	0.48368	0.51934	0.55807	0.60026	0.64638	0.69699	0.75278	0.81455	0.8833	0.96027	1.04699	1.14542	1.25806	1.3882	1.5402
	3.4	0.30643	0.32909	0.35333	0.37932	0.40724	0.4373	0.46976	0.5049	0.54306	0.58462	0.63007	0.67994	0.7349	0.79576	0.8635	0.93934	1.02479	1.12177	1.23275	1.36098
	3.45	0.27436	0.29528	0.31761	0.3415	0.36711	0.39463	0.42426	0.45625	0.49088	0.52848	0.56945	0.61423	0.66338	0.71754	0.77752	0.84428	0.91902	1.00323	1.0988	1.20818
	3.5	0.24449	0.26383	0.28445	0.30646	0.33001	0.35526	0.38238	0.41159	0.44312	0.47725	0.51432	0.5547	0.59884	0.64729	0.70068	0.75981	0.82561	0.89928	0.98228	1.07649
	3.55	0.21661	0.23453	0.2536	0.27393	0.29563	0.31885	0.34374	0.37048	0.39927	0.43036	0.46401	0.50056	0.54037	0.58389	0.63166	0.6843	0.74259	0.80747	0.8801	0.96193
	3.6	0.19053	0.20717	0.22485	0.24365	0.2637	0.2851	0.30799	0.33254	0.3589	0.3873	0.41795	0.45114	0.48718	0.52644	0.56936	0.61646	0.66837	0.72585	0.78982	0.86145
	3.65	0.16612	0.18159	0.19799	0.21543	0.23398	0.25375	0.27485	0.29744	0.32164	0.34765	0.37565	0.40589	0.43862	0.47417	0.51289	0.55522	0.60167	0.65287	0.70956	0.77266
	3.7	0.14321	0.15762	0.17288	0.18907	0.20626	0.22456	0.24406	0.26489	0.28716	0.31104	0.3367	0.36432	0.39415	0.42644	0.46151	0.4997	0.54146	0.58729	0.6378	0.69372
	3.75	0.1217	0.13513	0.14935	0.1644	0.18038	0.19734	0.2154	0.23464	0.25518	0.27716	0.30073	0.32604	0.3533	0.38273	0.41459	0.44918	0.48687	0.52807	0.57329	0.62312
	3.8	0.10146	0.11401	0.12727	0.14129	0.15615	0.17191	0.18866	0.20647	0.22546	0.24574	0.26743	0.29068	0.31566	0.34256	0.3716	0.40304	0.43718	0.47438	0.51503	0.55966
	3.85	0.0824	0.09413	0.10652	0.11961	0.13345	0.14811	0.16367	0.1802	0.19778	0.21653	0.23654	0.25795	0.28089	0.30555	0.3321	0.36077	0.3918	0.4255	0.46221	0.50234
	3.9	0.06442	0.07541	0.08699	0.09922	0.11214	0.12581	0.14028	0.15564	0.17195	0.18931	0.20782	0.22757	0.24871	0.27136	0.2957	0.32191	0.35021	0.38084	0.41411	0.45035
	3.95	0.04744	0.05775	0.0686	0.08004	0.09211	0.10486	0.11836	0.13265	0.14781	0.16392	0.18106	0.19933	0.21883	0.2397	0.26207	0.2861	0.31198	0.33992	0.37017	0.40301
	4	0.0314	0.04107	0.05124	0.06196	0.07325	0.08517	0.09777	0.11109	0.12521	0.14018	0.15609	0.17301	0.19105	0.21031	0.23092	0.25301	0.27674	0.30229	0.32988	0.35975
	4.05	0.01621	0.02529	0.03485	0.0449	0.05548	0.06663	0.07841	0.09085	0.10401	0.11795	0.13274	0.14845	0.16516	0.18298	0.202	0.22236	0.24417	0.26761	0.29285	0.3201
	4.1	0.00182	0.01037	0.01934	0.02878	0.0387	0.04916	0.06018	0.07181	0.0841	0.0971	0.11087	0.12548	0.14099	0.15751	0.17511	0.1939	0.214	0.23555	0.2587	0.28364
	4.15	-0.0118	-0.0038	0.00467	0.01354	0.02286	0.03266	0.04299	0.05388	0.06537	0.07751	0.09035	0.10396	0.11839	0.13372	0.15003	0.16742	0.18599	0.20585	0.22714	0.25001
	4.2	-0.0248	-0.0172	-0.0092	-0.0009	0.00787	0.01708	0.02677	0.03697	0.04773	0.05908	0.07108	0.08377	0.09721	0.11147	0.12662	0.14274	0.15992	0.17826	0.19789	0.21893
	4.25	-0.0371	-0.0299	-0.0224	-0.0146	-0.0063	0.00233	0.01143	0.02101	0.03109	0.04172	0.05294	0.0648	0.07734	0.09062	0.10471	0.11969	0.13562	0.15259	0.17072	0.19012
	4.3	-0.0488	-0.042	-0.035	-0.0276	-0.0198	-0.0116	-0.0031	0.00592	0.01538	0.02535	0.03586	0.04695	0.05866	0.07106	0.08419	0.09812	0.11291	0.12866	0.14544	0.16336
	4.35	-0.0599	-0.0536	-0.0469	-0.0399	-0.0326	-0.0249	-0.0168	-0.0084	0.00053	**0.00989**	0.01974	0.03013	0.04109	0.05267	0.06492	0.0779	0.09167	0.1063	0.12186	0.13845
	4.4	-0.0706	-0.0645	-0.0582	-0.0516	-0.0447	-0.0374	-0.0299	-0.0219	-0.0135	-0.0047	0.00452	0.01426	0.02452	0.03536	0.04681	0.05893	0.07176	0.08537	0.09983	0.11522

Table 4.3 (b) : Test Case Numerical results of Max_b
for $2.90 < T < 4.40$ and $1.80 < p < 2.75$

Findings in this section reveal that the method discussed has indeed optimized the time while setting the cable tensions at the minimum values possible.

5. CONCLUSION

This report presented a simple, yet an effective analytical method to circumvent the cable tension determination problem and design a time optimized point – to –point straight line trajectory with smooth dynamics for redundantly actuated 2DoF (planer) and 3DoF (spatial) CSPRs while ensuring positive cable tensions. The FAD model which enables to perceive the feasibility of motion of CSPR as a relationship between potential accelerations and the position is the key to develop this new methodology. Major concepts exclusively developed in this research are the FAD diagrams and the S-model. Since this is an analytical method highly accurate results can be obtained while determining of the motion parameters, which has been confirmed during the simulation of results.

The method developed is simple and does not include any numerical method or an exhaustive search algorithm to obtain results. Thus, will use very low resources of a controller which may be programmed to determine the motion parameters. Since in this method, all the motion parameters will be calculated prior to initializing the motion, controller can be programmed to first calculate the motion parameters and then use its resources to control the motion using a standard control technique such as PID. Which leads to better management of controller resources.

This research can be extended into several areas. In case of avoiding obstacles, a single straight-line trajectory can be slightly modified to have series of straight lines. The method developed in this thesis can still be used to develop series of time optimized straight lines to move from initial position to final position. However, the optimization can further be enhanced by allowing non-zero accelerations at intermediate points between straight lines. The research has considered a straight-line trajectory as its path, and a kinematic model of continuous increase of velocity followed by a continuous decrease of the same. Variations of the path as well as the model can be tested to fine tune the optimizations.

REFERENCE LIST

[1] C. Gosselin and S. Foucault, "Dynamic Point-to-Point Trajectory Planning of a Two-DOF Cable-Suspended Parallel Robot," *IEEE Transactions on Robotics*, vol. 30, no. 3, June 2014.

[2] . J. Xiaoling and C. Gosselin, "Trajectory Generation for Three-Degree of Freedom Cable Suspended parallel Robots Based on Analytical integration of Dynamic Equations," *Journal of Mechanisms and Robotics,* vol. 8, no. August, 2016.

[3] G. Mottola, C. Gosselin and M. Carricato, "Dynamically-Feasible Elliptical Trajectories for Fully Constrained 3-DOF Cable-Suspended Parallel Robots," *Mechanisms and Machine Science,* 2018.

[4] G. Mottola, C. Gosselin and M. Carricato, "Dynamically Feasible Periodic Trajectories for Generic Spatial 3-DOF Cable-Suspended Parallel Robots," *Journal of Mechanisms and Robotics*, March 2018.

[5] C. Gosselin, "Global Planning of Dynamically Feasible Trajectories for Three-DOF Spatial Cable-Suspended Parallel Robots," in *Mechanisms and Machine Science*, Berlin Heidelberg, Springer-Verlag, 2013.

[6] Y. Su, Y. Qiu and P. Liu, "The continuity and real-time performance of the cable tension determining for a suspend cable-driven parallel camera robot," in *Advanced Robotics*, Taylor & Francis, Taylor & Francis, 2015.

[7] J. Lamaury and M. Gouttefarde, "A Tension Distribution Method with Improved Computational Efficiency," in *Mechanisms and Machine Science*, Berlin Heidelberg, Springer-Verlag, 2013.

[8] J. Lamaury and and M. Gouttefarde, "Control of a Large Redundantly Actuated Cable-Suspended Parallel Robot," in *IEEE International Conference on Robotics and Automation (ICRA)*, Karlsruhe, 2013.

[9] P. Bosscher, A. T. Riechel and I. Ebert-Uphoff, "Wrench-Feasible Workspace Generation for Cable-Driven Robots," *IEEE Transactions for Robotics,* vol. 22, no. 5, October 2006.

[10] C. Gosselin, P. Ren and S. Foucault, "Dynamic Trajectory Planning of a Two-DOF Cable-Suspended Parallel," in *IEEE International Conference on Robotics and Automation,* Saint Paul, 2012.

[11] A. Berti, J.-P. Merlet and M. C., "Solving the direct geometrico-static problem of underconstrained cable-driven parallel robots by interval analysis," *The International Journal of Robotics Research,* 2015.

[12] G. Abbasnejad and M. Carricato, "Direct Geometrico-static Problem of Underconstrained Cable-Driven Parallel RobotsWith n Cables," *IEEE Transactions on Robotics,* vol. 31, no. 2, April 2015.

[13] X. Jiang and C. Gosselin, "Dynamically Feasible Trajectories for 3DoF Planar Cable Suspended Parallel Robots," in *ASME 2014 International Design Engineering Technical Conferences & Computers and Information in Engineering Conference*, Buffalo, 2014.

[14] A. T. Riechel and I. E. Uphoff, "Force-Feasible Workspace Analysis for Underconstrained, Point-Mass Cable Robots," in *IEEE Internatlonal Conference on Robotics & Automation*, New Orleans, 2004.

[15] E. Ottaviano, V. Gattulli and F. P., "Elasto-Static Model for Point Mass Sagged Cable-Suspended Robots," in *Springer Proceedings in Advanced Robotics 4*, 2018.

APPENDIX A: DEDUCTION OF INEQUALITIES FOR FEASIBLE TRAJECTORIES

PART 1: Deduction of Lower Boundary Lines of FAD in 2DOF, 2 Cable Configuration.

Refer figure 2.1 and figure 2.2.

Case 1: Equation of the line 1.D.

Say the vector $\frac{T_1}{m}$along the cable 1 contributing to the resultant acceleration is$\lambda\frac{T_{1,max}}{m}$, where λa constant is. Considering the relevant vectors of diagram:

$$[\ddot{x} \quad \ddot{z}]^T = -g + \frac{T_1}{m} = [0 \quad -g]^T + \lambda\frac{T_{1,max}}{m}[-x \quad (z_{max} - z)]^T$$

Therefore,

$$\ddot{x} = \lambda(-x)\,;\ddot{z} = \lambda(z_{max} - z) - g$$

Eliminating $\lambda\frac{T_{1,max}}{m}$ from above, the Equation of Line 1.D:

$$\ddot{z} = \frac{(z_{max}-z)}{-x}\ddot{x} - g$$

Case 2: Equation of the line 2.D.

Say the vector $\frac{T_2}{m}$along the cable 2 contributing to the resultant acceleration is $\gamma\frac{T_{2,max}}{m}$, where varying values of γ gives different points in line. Considering the relevant vectors of diagram:

$$[\ddot{x} \quad \ddot{z}]^T = -g + \frac{T_2}{m} = [0 \quad -g]^T + \gamma\frac{T_{2,max}}{m}[(x_{max} - x) \quad (z_{max} - z)]^T$$

Therefore,

$$\ddot{x} = \gamma(x_{max} - x)\,;\ddot{z} = \gamma\frac{T_{2,max}}{m}(z_{max} - z) - g$$

Eliminating γ from above, the equation of line 2.D:

$$\ddot{z} = \frac{(z_{max}-z)}{(x_{max}-x)}\ddot{x} - g$$

PART 2: Deduction of Boundary planes of FAD in 3-DOF, 4-Cable Configuration.

Consider the configuration of any two cables in a 3DoF configuration given in figure A.1:

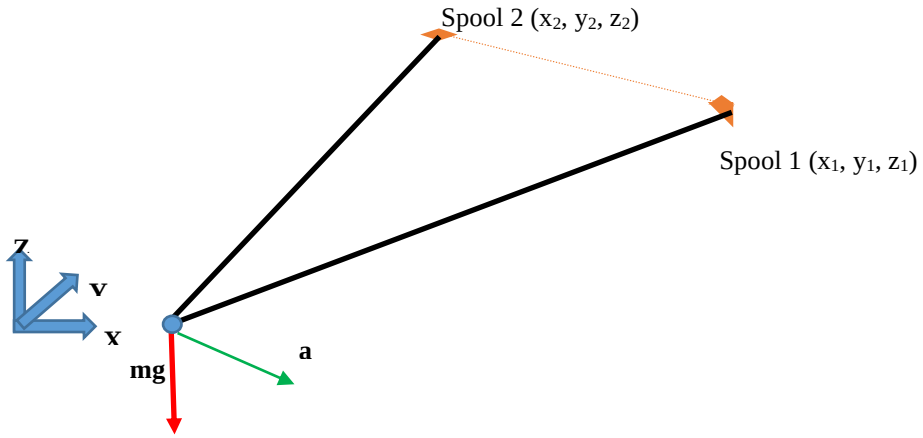

Figure A.1: General configuration of any two cables in a 3DoF case.

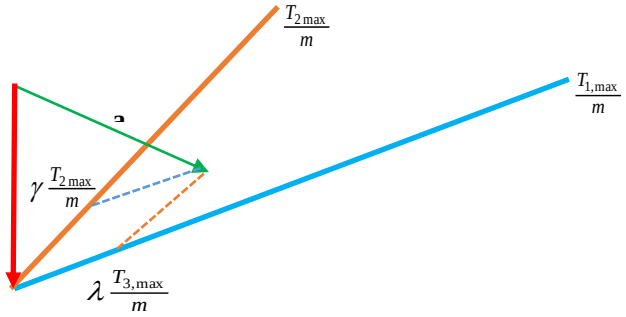

Figure A.2: Portion of FAD corresponding to cable directions in figure A.1

Say the vector $\frac{T_1}{m}$ along the cable 1 contributing to the resultant acceleration is $\lambda \frac{T_{1,max}}{m}$, and vector $\frac{T_2}{m}$ along the cable 2 contributing to the resultant acceleration is $\gamma \frac{T_{2,max}}{m}$where varying values of λandγgives different points in plane generated by vectors $\frac{T_{1,max}}{m}$and $\frac{T_{2,max}}{m}$. Considering the relevant vectors of diagram:

$$[\ddot{x} \quad \ddot{y} \quad \ddot{z}]^T =$$

$$[0 \quad 0 \quad -g]^T + \lambda \frac{T_{1,\max}}{m}[(x_1 - x) \quad (y_1 - y) \quad (z_1 - z + g)]^T + \gamma \frac{T_{2,\max}}{m}[(x_2 - x) \quad (y_2 - y) \quad (z_2 - z + g)]^T$$

Therefore,

$$\ddot{x} = \lambda \frac{T_{1,max}}{m}(x_1 - x) + \gamma \frac{T_{2,max}}{m}(x_2 - x);$$

$$\ddot{y} = \lambda \frac{T_{1,max}}{m}(y_1 - y) + \gamma \frac{T_{2,max}}{m}(y_2 - y);$$

$$\ddot{z} = -g + \lambda \frac{T_{1,max}}{m}(z_1 - x) + \gamma \frac{T_{2,max}}{m}(z_2 - x);$$

Eliminating $\lambda \frac{T_{1,max}}{m}$ and $\gamma \frac{T_{2,max}}{m}$ from above, and substituting $z_1 = z_2$ following equation of the plane can be obtained:

$$\ddot{z} = \frac{\ddot{x}(y_2 - y_1)(z_1 - z) - \ddot{y}(x_2 - x_1)(z_1 - z)}{\{y_2(x_1 - x) - y_1(x_2 - x) + y \quad (x_2 - x_1)\}} - g$$

Refer figure 2.7 for the remaining section of this part.

Case-1: Equation of the plane generated by T_1 and T_2 vectors

Substituting values for $x_1 = 0$, $y_1 = 0$, $z_1 = z_{max}$, $x_2 = x_{max}$, $y_2 = 0$, $z_2 = z_{max}$; following equation of the plane can be obtained:

$$\ddot{z} = \left(\frac{z_{max} - z}{-y}\right)\ddot{y} - g$$

Case-2: Equation of the plane generated by T_2 and T_3 vectors

Substituting values for $x_1 = x_{max}$, $y_1 = 0$, $z_1 = z_{max}$, $x_2 = x_{max}$, $y_2 = y_{max}$, $z_2 = z_{max}$; following equation of the plane can be obtained:

$$\ddot{z} = \left(\frac{z_{max} - z}{x_{max} - x}\right)\ddot{x} - g$$

Case-3: Equation of the plane generated by T_3 and T_4 vectors

Substituting values for $x_1 = x_{max}$, $y_1 = y_{max}$, $z_1 = z_{max}$, $x_2 = 0$, $y_2 = y_{max}$, $z_2 = z_{max}$; following equation of the plane can be obtained:

$$\ddot{z} = \left(\frac{z_{max} - z}{y_{max} - y}\right)\ddot{y} - g$$

Case-4: Equation of the plane generated by T_3 and T_4 vectors

Substituting values for $x_1 = x_{max}$, $y_1 = y_{max}$, $z_1 = z_{max}$, $x_2 = 0$, $y_2 = y_{max}$, $z_2 = z_{max}$; following equation of the plane can be obtained:

$$\ddot{z} = \left(\frac{z_{max} - z}{-x}\right)\ddot{x} - g$$

APPENDIX B: PROOF SUPPORTING THE DETERMINATION OF Q POINTS

This annexure contains the proof of expression "since $\ddot{s}(t)$ is piecewise linear in t between odd points R_i (I = 1, 3, 5, 7, 9) above, a curve drawn: $\ddot{s}(t)$ vs.$s(t)$ also lies inside the respective triangles (Q_1, Q_2, Q_3), (Q_3, Q_4, Q_5), (Q_5, Q_6, Q_7) and (Q_7, Q_8, Q_9) at all times, where q_i = { $s(t)$,$\ddot{s}(t)$, i=1..9} given in chapter 3.

Proof :

Say Q_i, Q_j and Q_k are set of three points in corners of a one of four triangles in above. Figure B.1 is an illustration of these on an s(t) and an $\ddot{s}$ (t) graph.

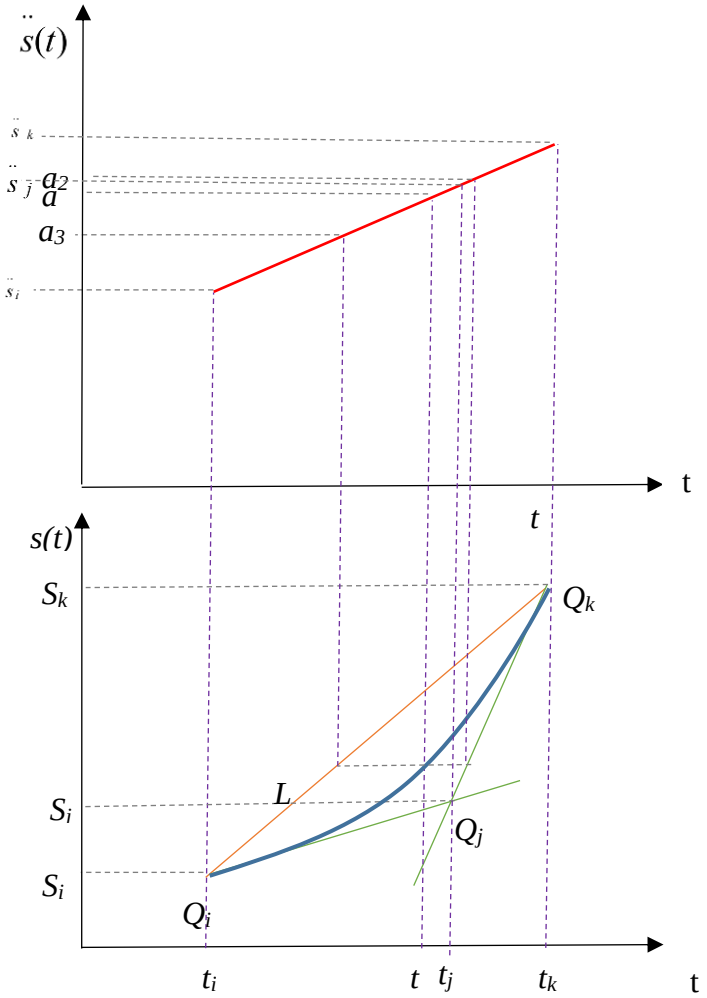

Figure B.1: Illustration of Q_i, Q_j and Q_k points

Refer the points given in figure B.1. Thick blue line refers to the actual function of s(t). Green lines are the tangents to s(t) at Q_i and Q_k . Note that both tangent parts Q_i – Q_j and Q_j – Q_k are linear and thus have linear relationships with relevant parts of $\ddot{s}(t)$ curve. Similarly the line Q_i – Q_k is also having a linear relationship with$\ddot{s}(t)$. Suppose these relationships are $\ddot{s} = f_1(s), \ddot{s} = f_2(s), \ddot{s} = f_3(s)$ respectively, and the actual relationship between s and $\ddot{s}$ is $\ddot{s} = f(s)$

Refer to any actual s(t) value at time t.
Note that $a_3 < a < a_2$.
However, $a_3 = f_3(s)$, $a = f\ (s)$ and $a = f_2(s)$.
Therefore, for any t, $f_3(s) < f\ (s) < f_2(s)$.

Similarly it can be proven that, $f_3(s) < f\ (s) < f_1(s)$
This proves that any point in $\ddot{s} = f(s)$ are bound by functions $f_1(s), f_2(s), f_3(s)$. which are essentially defined by points,$(s_i, \ddot{s}_i)$,$(s_j, \ddot{s}_j)$ and$(s_k, \ddot{s}_k)$. This can similarly be proven for a curve of reducing gradient.

APPENDIX C: CALCULATION OF 'TENSION COUPLES'

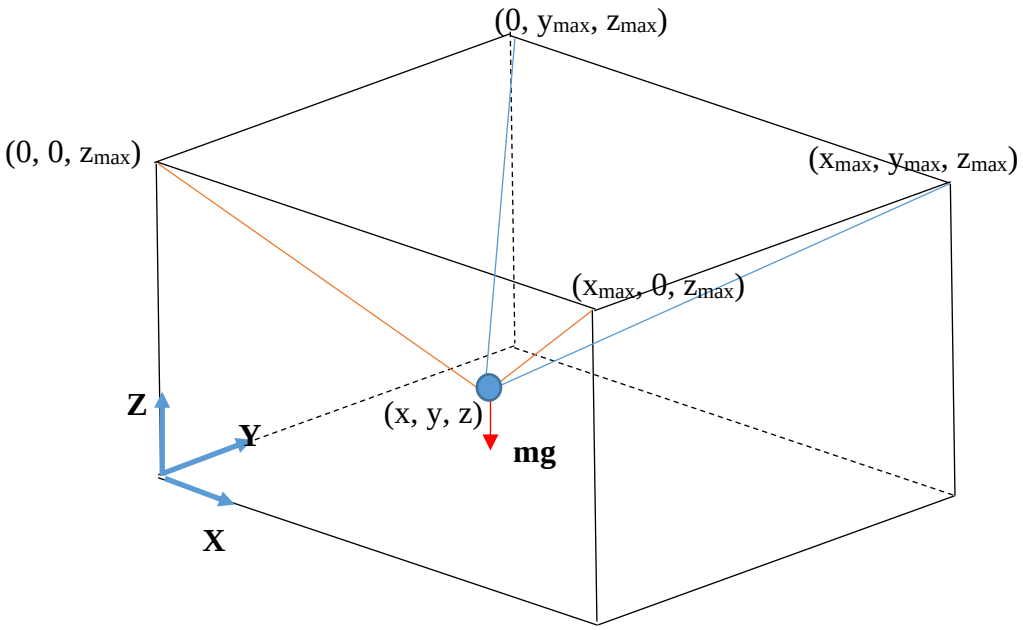

Figure C.1 : Illustration of Tension couples

Consider the Y-Z component of resultant tension of cables connecting points (0, y_{max}, z_{max}) with (x, y, z) and (x_{max}, y_{max}, z_{max}) with (x, y, z) respectively. This component is labelled as $T_{3,4.}$ Consider the Y-Z component of resultant tension of cables connecting points (0, 0, z_{max}) with (x, y, z) and (x_{max}, 0, z_{max}) with (x, y, z) respectively. This component is labelled as $T_{1,2.}$ These components will be referred to as 'Tension couples'.

For the acceleration in Y direction :

$$-T_{1,2}.\frac{y}{\sqrt{y^2+(z_{max}-z)^2}}+T_{3,4}.\frac{y}{\sqrt{(y_{max}-y)^2+(z_{max}-z)^2}}=m\ddot{y}$$

For the acceleration in Z direction :

$$T_{1,2}.\frac{(z_{max}-z)}{\sqrt{y^2}+(z_{max}-z)^2}+T_{3,4}.\frac{(z_{max}-z)}{\sqrt{(y_{max}-y)^2}+(z_{max}-z)^2}-mg=m\ddot{z}$$

Solving above equations yield the values:

$$T_{1,2}. = \frac{[-\ddot{y}(z_{max} - z) + (\ddot{z} + g)(y_{max} - y)]\sqrt{y^2 + (z_{max} - z)^2}}{y_{max}(z_{max} - z)}$$

$$T_{3,4}. = \frac{[\ddot{y}(z_{max} - z) + (\ddot{z} + g)(y_{max} - y)]\sqrt{(y_{max} - y)^2 + (z_{max} - z)^2}}{y_{max}(z_{max} - z)}$$

Similarly, $T_{2,3}$ and $T_{4,1}$ were found as:

$$T_{2,3}. = \frac{[\ddot{x}(z_{max} - z) + (\ddot{z} + g)(x_{max} - x)]\sqrt{(x_{max} - x)^2 + (z_{max} - z)^2}}{u(w - z)}$$

$$T_{4,1}. = \frac{[-\ddot{x}(z_{max} - z) + (\ddot{z} + g)(x_{max} - x)]\sqrt{(x_{max} - x)^2 + (z_{max} - z)^2}}{x_{max}(w - z)}$$